

1 **TITLE:**
2 A shift from pleiotropic to modular adaptation revealed by a high-resolution two-step adaptive
3 walk

4
5 **AUTHORS:**
6 Grant Kinsler^{1,2}, Yuping Li^{3,4}, Gavin Sherlock^{*,3}, Dmitri A. Petrov^{*,1}

7
8 **AFFILIATIONS:**
9 ¹Department of Biology, Stanford University
10 ²Department of Bioengineering, University of Pennsylvania
11 ³Department of Genetics, Stanford University
12 ⁴Department of Microbiology & Immunology, UC San Francisco
13 *Equal contribution
14

15 **ABSTRACT:**
16
17 Evolution by natural selection is expected to be a slow and gradual process. In particular, the
18 mutations that drive evolution are predicted to be small and modular, incrementally improving a
19 small number of traits. However, adaptive mutations identified early in microbial evolution
20 experiments, cancer, and other systems often provide substantial fitness gains and
21 pleiotropically improve multiple traits at once. We asked whether such pleiotropically adaptive
22 mutations are common throughout adaptation or are instead a rare feature of early steps in
23 evolution that tend to target key signaling pathways. To do so, we conducted barcoded second-
24 step evolution experiments initiated from five first-step mutations identified from a prior yeast
25 evolution experiment. We then isolated hundreds of second-step mutations from these evolution
26 experiments, measured their fitness and performance in several growth phases, and conducted
27 whole-genome sequencing of the second-step clones. Here, we found that while the vast
28 majority of mutants isolated from the first-step of evolution in this condition show patterns of
29 pleiotropic adaptation - improving both performance in fermentation and respiration growth
30 phases - second-step mutations show a shift towards modular adaptation, mostly improving
31 respiration performance and only rarely improving fermentation performance. We also identified
32 a shift in the molecular basis of adaptation from genes in cellular signaling pathways towards
33 genes involved in respiration and mitochondrial function. Our results suggest that the genes in
34 cellular signaling pathways are particularly capable of providing large, adaptively pleiotropic
35 benefits to the organism due to their ability to coherently affect many phenotypes at once. As
36 such, these genes may serve as the source of pleiotropic adaptation in the early stages of
37 evolution, and once these become exhausted, organisms then adapt more gradually, acquiring
38 smaller, more modular mutations.

39 **INTRODUCTION**

40
41 As organisms adapt to their environment, they face a multi-dimensional optimization problem.
42 To be advantageous, new mutations must improve one or more traits under selection without
43 imposing strong costs on other traits. Theoretical analyses of adaptive walks in multi-
44 dimensional trait spaces suggest that mutations that generate small phenotypic shifts in few
45 traits are more likely to be beneficial overall than mutations of large phenotypic effect on many
46 traits (Orr 2000). Consequently, adaptive mutations are expected to both provide small fitness
47 benefits and to be **modular** – that is, affect only a few traits without affecting others.

48
49 Despite these theoretical expectations, microbial evolution experiments have revealed that early
50 adaptation often proceeds by single mutations that provide large fitness benefits (Y. Li, Petrov,
51 and Sherlock 2019; Wiser, Ribeck, and Lenski 2013; Levy et al. 2015; Johnson et al. 2021;
52 Venkataram et al. 2016). Moreover, in the cases where the improvement of these mutations has
53 been decomposed into distinct trait performances, it is often observed that these mutations
54 improve multiple traits simultaneously (as illustrated in Figure 1A) (Y. Li, Petrov, and Sherlock
55 2019; Y. Li et al. 2018; Bono et al. 2017; Jasmin and Kassen 2007).

56
57 The observation of adaptive mutations improving multiple performances at once, which we here
58 term “**pleiotropic adaptation**”, can be easily seen in a series of evolution experiments
59 conducted with barcoded yeast in which a comprehensive set of adaptive mutations was
60 profiled for their effects on likely orthogonal trait performances (Levy et al. 2015; Venkataram et
61 al. 2016; Y. Li, Petrov, and Sherlock 2019; Y. Li et al. 2018). Li et al (2018) in particular showed
62 that ~85% of first-step adaptive mutations isolated from their evolution experiment improve
63 performance in both fermentation and respiration growth phases, both of which are under
64 selection during the yeast growth cycle. These pleiotropic mutants from this initial step of
65 adaptation, many of which harbor only a single mutation in the Ras/PKA pathway, are also
66 strongly adaptive, providing fitness benefits of up to 120% per growth cycle (roughly 15% per
67 generation) (Venkataram et al. 2016). Such large-effect Ras/PKA pathway mutations are
68 commonly found in early evolution in other systems, such as cancer progression (Bailey et al.
69 2018). As the study we present here follows on from our previous series of findings, we use
70 these yeast mutations as a motivating example throughout the rest of the introduction.

71
72 How do we reconcile our observations of pleiotropic adaptation (Y. Li et al. 2018) with
73 theoretical expectations that these mutations should affect only a small number of traits? One
74 possibility is that fermentation and respiration performances are not as distinct as we believe.
75 However, a number of adaptive mutations do improve only one of these performances,
76 demonstrating that it is in fact possible to shift one performance without affecting the other.

77
78 The other possibility is that the Ras/PKA pathway is wired in such a way that mutations that
79 target this pathway are capable of being both pleiotropic and adaptive, affecting many
80 phenotypes of the organism but in a coherent and coordinated fashion. It might be that

81 mutations in general might not have these patterns of pleiotropic adaptation and instead exhibit
82 “**modular adaptation**”, improving only a subset of the traits under selection. Thus, isolating and
83 characterizing the effects of subsequent mutations, which may be less likely to target this
84 already-mutated pathway, might better reflect the pleiotropic properties of adaptive mutations
85 beyond these extremely beneficial first-step mutations in the Ras/PKA pathway. One way in
86 which we can assess whether the observed adaptive pleiotropy is a common feature of adaptive
87 mutations is to conduct adaptive walks, evolving populations further in the same environment.
88 We can then ask whether later adaptive mutations continue to show pleiotropic adaptation or
89 not.

90
91 One possibility is that pleiotropic adaptation is indeed common. This may be true if there are
92 many pathways in the cell that can be mutated to yield simultaneous improvement of the traits
93 under selection or, instead, if the signaling pathways mutated early can continue to be optimized
94 beyond the first adaptive step. In this scenario, second-step adaptive mutations would continue
95 to improve both traits under selection (Figure 1B, red points) and longer adaptive walks would
96 also continue to show this pattern of pleiotropic adaptation (Figure 1B arrows).

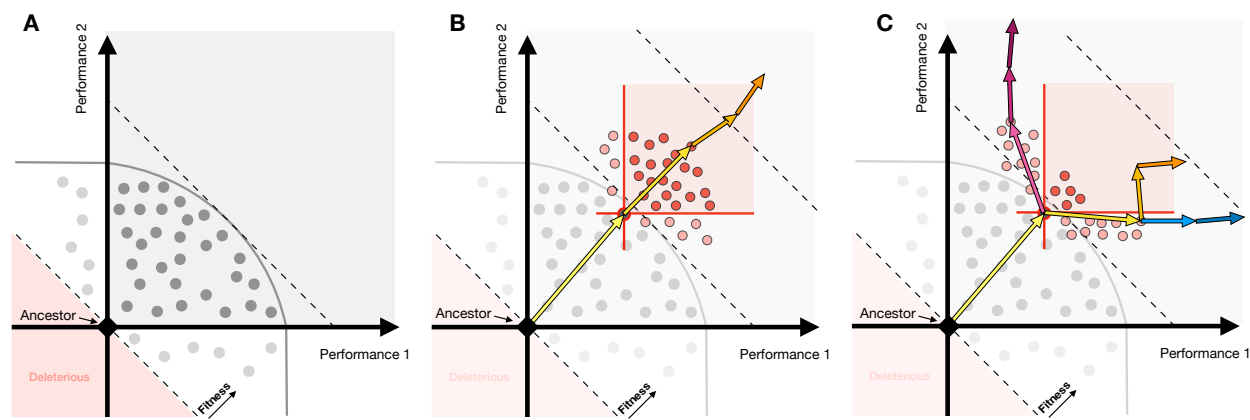
97
98 Alternatively, pleiotropic adaptation may be rare, and first-step mutations target the only (or one
99 of few) signaling pathway(s) which can result in simultaneous improvement of multiple traits
100 (performance in both fermentation and respiration growth phases in the case of the yeast
101 evolution experiments). For adaptation to continue, it would need to engage the modules that
102 can independently control the performance in each growth phase. Individual second-step
103 mutations under this scenario would then be expected to exhibit a pattern of “modular
104 adaptation”, improving only one performance under selection or the other (Figure 1C). The
105 longer adaptive walks could continue down this route of specialization in either a single
106 performance (blue or magenta arrows) or instead improve both performances under selection,
107 but via sequential improvement of one performance and then the other (orange arrows).

108
109 Thus, to characterize the nature of single-step adaptive mutations and whether the observation
110 of pleiotropic adaptation of first-step mutations is a general feature of individual adaptation-
111 driving mutations or instead a rare feature of early adaptive mutations, we need to
112 experimentally conduct high-resolution adaptive walks, wherein we can isolate adaptive
113 mutations, quantify their effects on traits relevant to fitness, and identify the molecular basis of
114 adaptation. The yeast barcoding system developed by (Levy et al. 2015) is particularly well-
115 suited for this set of experiments, as we can isolate hundreds of mutations per evolution
116 experiment and study their properties via pooled fitness measurement experiments.

117
118 In this study, we perform second-step evolution experiments using a set of five first-step
119 adaptive mutations isolated from a glucose-limited evolution experiment (Levy et al. 2015) as
120 new ancestors. We then isolate hundreds of mutants from these evolution experiments and
121 measure their performance in the growth phases that make up the evolution condition. We find
122 a shift in the nature of adaptation over this two-step adaptive walk. While first-step mutations

123 primarily demonstrate pleiotropic adaptation, improving performance in both growth phases
 124 under selection, second-step mutations instead primarily exhibit modular adaptation, improving
 125 performance in only a single growth phase under selection (Figure 1C). Whole genome
 126 sequencing reveals an associated shift in the molecular basis of adaptation: from first-step
 127 mutations in general signaling pathways to second-step mutations in genes related to
 128 mitochondrial function and respiration. Finally, we sample rare adaptive clones that showed
 129 patterns of adaptive pleiotropy and discovered that they harbor multiple additional mutations.
 130 This suggests that these populations have not yet reached physiological constraints but rather
 131 that adaptive walks may be constrained by genetic modules which prevent adaptive mutations
 132 from improving multiple performances in a single step.
 133

134 This shows that early adaptation, here represented by the first-step in our evolution experiment,
 135 can engage signaling pathways that allow for rapid, large step pleiotropic adaptation but later
 136 adaptation is more likely to be modular, as expected by theory. We thus expect that longer term
 137 evolution will indeed progress through smaller, and ultimately more modular, adaptive
 138 mutations.



139
 140 **Figure 1. Theoretical illustration: Pleiotropy may be a generic feature of adaptation or specific to**
 141 **the first-step of evolution. (A)** First-step adaptive mutations (each mutation depicted as a dot) in
 142 evolution often exhibit patterns of pleiotropic adaptation - improving performance in multiple traits
 143 simultaneously (falling into the gray square). Gray curved line represents the limits of combinations of
 144 performances reached by the first-step of evolution. **(B)** If pleiotropic adaptation is common, then second-
 145 step adaptive mutations (depicted in red) would continue to improve multiple performances at once.
 146 Longer adaptive walks would also continue to show these patterns (orange arrows). **(C)** If pleiotropic
 147 adaptation is rare and largely constrained to the first adaptive step, then second-step adaptive mutations
 148 might show a shift in their improvement, instead primarily improving one performance or the other (light
 149 red circles). In this scenario, longer term adaptive walks may continue to specialize in one performance or
 150 the other (depicted by blue and magenta arrows), or instead continue to collectively improve both
 151 performances, albeit in a stepwise manner (orange arrows).

152 **RESULTS**

153

154 **Isolating second-step adaptive clones and measuring performance in growth phases**

155

156 When yeast are grown in an environment under glucose-limitation in batch culture, they
157 experience several growth phases (Figure 2A). First, the yeast experience lag phase, where
158 they acclimate to the environment and allocate cellular resources to consuming glucose. Then,
159 the yeast ferment the glucose, converting it to ethanol. Once the glucose is consumed, the
160 yeast then undergo the diauxic shift and respire on the ethanol they produced during
161 fermentation. Finally, once the supply of ethanol has been depleted, the yeast experience
162 stationary phase, where they allocate resources to surviving without a carbon source. These
163 growth phases are typically thought of as independent processes, with distinct transcriptional,
164 proteomic, and metabolomic profiles that characterize and drive yeast physiology (DeRisi, Iyer,
165 and Brown 1997; Schlossarek et al. 2022; Zampar et al. 2013; Murphy et al. 2015).

166

167 Previously, a population of barcoded yeast was evolved in a 2-Day transfer environment under
168 glucose limitation, where they experienced lag, fermentation, and respiration but not stationary
169 phases before being transferred to fresh medium (Levy et al. 2015; Venkataram et al. 2016).
170 Adaptive mutations isolated from this experiment gained substantial fitness benefits, primarily by
171 constitutively activating one of two glucose-sensing pathways: Ras/PKA and TOR/Sch9
172 (Venkataram et al. 2016). Additionally, 85% of these mutants improved performance in both
173 fermentation and respiration phases, despite the supposed independence of these growth
174 phases. Interestingly, with additional evolution experiments designed to maximize individual
175 performances, Li et al (2019) were able to find evidence of constraints on the first step of
176 evolution such that no single mutation is able to simultaneously maximize both fermentation and
177 respiration performances to the largest extreme of each performance observed individually.

178

179 To understand whether pleiotropic adaptation is common or if instead first-step mutations
180 represent rare solutions that improve both traits under selection, we carried out second-step
181 evolution experiments in the same 2-Day transfer environment, isolated adaptive mutants,
182 identified causative mutations underlying adaptation, and characterized the mutations' effects
183 on performance in the environment's growth phases. Aggeli et al. (Aggeli, Li, and Sherlock
184 2021) previously performed second-step evolution experiments using barcoded populations that
185 carried one of three mutations identified in the first step of evolution: a gain-of-function mutation
186 in *CYR1*, a loss-of-function mutation in *GPB2*, and a gain-of-function mutation in *TOR1*. Here,
187 we used additional barcoded populations derived from two distinct mutations in *IRA1*: one
188 missense mutation and one nonsense mutation (see Methods). We then evolved 2 replicates of
189 each barcoded population in the 2-Day transfer condition, labeled here "Evo2D", for 22 transfers
190 (~176 generations) and isolated adaptive clones (Figure 2B,C). As we were also interested in
191 how the number of traits under selection alters the extent of pleiotropic adaptation, we also
192 evolved the same barcoded populations in a 3-Day transfer condition, herein termed "Evo3D",
193 where populations experienced an additional 12 hours of respiration and 12 hours of stationary

194 phase, and isolated adaptive clones from this additional set of evolution experiments (Figure
195 2A-C; see Methods).

196

197 To assess the extent to which physiological and genetic constraints affect the second-step of
198 adaptation, we quantified each mutant's performance in fermentation, respiration, and stationary
199 growth phases using pooled barcoded fitness assays, as developed previously (Figure 2B;
200 (Venkataram et al. 2016; Y. Li et al. 2018; Y. Li, Petrov, and Sherlock 2019; Kinsler, Geiler-
201 Samerotte, and Petrov 2020; Kinsler et al. 2023). Briefly, we pooled all isolated second-step
202 mutants together with the barcoded mutants from the first step of evolution. We then mixed this
203 pool of barcoded yeast with a set of barcoded neutral lineages and the ancestral strain, such
204 that the barcoded pool started at either 2% or 5% frequency in the population and the neutral
205 barcoded lineages collectively represented 2% of the population (see Methods). We then
206 measured the fitness of each mutant by serially transferring $\sim 5 \times 10^7$ cells for five cycles in 1-,
207 2-, 3-, and 5-Day transfer intervals. At each transfer, we froze down the remaining cells,
208 extracted their DNA, amplified the barcode region with PCR, and then sequenced the barcode
209 region. We then calculated each mutant's fitness relative to the ancestor by comparing each
210 mutant's frequency change with the pool of neutral lineages (Figure 2B, see Methods).

211

212 During the analysis of fitness measurement data, we observed that the detected fitness effects
213 of each mutant varied systematically over the course of serial transfers during the fitness
214 measurement of the isolated adaptive clones. Specifically, in the 2-Day transfer condition, many
215 adaptive mutants showed very high fitness when the ancestral strain was at or above 80% of
216 the population but showed much lower fitness at later time intervals when the pool of adaptive
217 lineages dominated the population. We note that this effect is not due to change in population
218 mean fitness, as this is already accounted for in these fitness values. While intriguing, we
219 avoided these frequency dependent fitness effects in our data by using only early timepoints,
220 where the ancestor dominated the population, as these reflect the fitness in the environment set
221 by the ancestor and where the fitness of mutants isolated from the original evolution experiment
222 matched their fitness measurements in previous experiments (Figure S1).

223

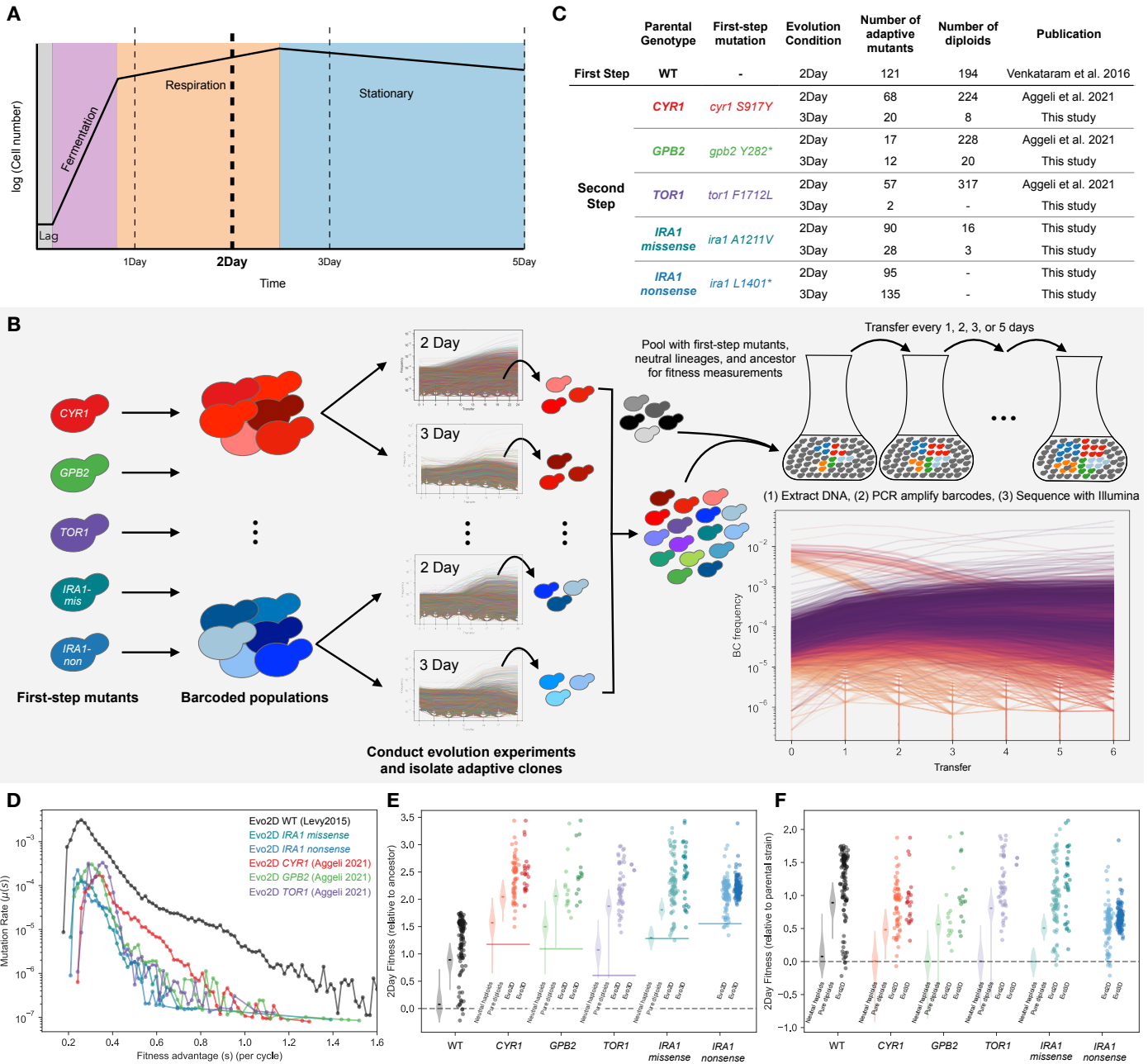
224 **Second-step adaptive mutations provide substantial yet smaller fitness benefits than**
225 **first-step mutations**

226

227 We sequenced the barcodes in these populations to monitor the dynamics of evolution and to
228 quantify the distribution of fitness effects. Using the approach implemented in software FitMut1
229 (Levy et al. 2015; F. Li, Tarkington, and Sherlock 2023), we quantified the distribution of fitness
230 effects for these populations and the original evolution experiment. Because auto-diploidization
231 is a common mode of adaptation in evolution experiments with haploid yeast, we also used a
232 benomyl assay to determine the ploidy of the isolated adaptive clones (Figure 2C). We then
233 categorized mutants according to their ploidy status and fitness across pooled fitness
234 measurement experiments as neutral haploids, pure diploids, adaptive haploids, or high-fitness
235 diploids (diploids that have additional beneficial mutations, see Methods).

236 We found that the rate of beneficial mutations is reduced in the second-step of evolution in the
237 2-Day environment, with adaptive mutations that provide fitness benefits of 1.0 or greater (per
238 cycle) becoming much rarer (Figure 2D). This is consistent with the patterns of diminishing
239 returns epistasis commonly observed in microbial evolution experiments (Wiser, Ribeck, and
240 Lenski 2013; Johnson et al. 2021; Aggeli, Li, and Sherlock 2021; Good and Desai 2015;
241 Wünsche et al. 2017; Chou et al. 2011; Kryazhimskiy et al. 2014). While we see this general
242 decrease in the magnitude of the fitness benefit of adaptive mutations, we nonetheless find that
243 many second-step adaptive mutations still have substantial fitness gains in the 2-Day transfer
244 evolution condition. Across all isolated second-step adaptive mutants (excluding auto-diploids
245 and neutral haploids), the average fitness benefit provided is 82% per cycle relative to the
246 parental strain. This is similar across mutants isolated from both 2- and 3-Day evolution
247 experiments (Figure 2E,F). We also sampled rare mutants with fitness advantages as high as or
248 even higher than the most extreme fitnesses observed in the first step of evolution. For
249 example, two mutants isolated from the Evo3D *IRA1-missense* evolution experiments provide a
250 benefit of ~200% above the parental *IRA1-missense* strain, which corresponds to a ~350%
251 fitness advantage per 2-Day cycle over the original ancestor strain (Figure 2E,F). As will be
252 discussed later, these extremely fit mutants represent rare and complex mutations, sometimes
253 consisting of up to four distinct adaptive mutations.

254
255 We also calculated the relative fitness improvement provided by auto-diploidization alone by
256 comparing the fitness of the pure diploid population to the neutral haploids for each parental
257 strain. Consistent with the pattern of diminishing epistasis observed from the evolution
258 trajectories, we find that the fitness benefit of auto-diploidization has decreased in the second
259 step of evolution from 95% per cycle in the first-step of evolution to 63% on average across all
260 second-step auto-diploids (Figure 2F). However, this number varied by parental strain, with
261 *TOR1* auto-diploids providing the largest fitness benefit of 81% per cycle and auto-diploids of
262 Ras/PKA parental strains providing fitness benefits of 55%, 48%, and 52% per cycle to *CYR1*,
263 *GPB2*, and *IRA1-missense*, respectively (Figure 2F). Surprisingly, we did not isolate any auto-
264 diploids from the *IRA1-nonsense* evolution experiments. We suspect this could be due to
265 differences in the fitness benefit provided by auto-diploidization to *IRA1-nonsense* strains
266 compared to other beneficial mutations in the same evolving population or reduced auto-
267 diploidization rate in this genetic background.



268 **Figure 2. Summary of experiments and fitness effects of isolated adaptive mutants.** (A) A
269 schematic of yeast growth phases under the nutrient conditions used in this study. The yeast experience
270 4 hours of lag phase, 16 hours of fermentation and 4 hours of respiration phase in the first 24 hours of
271 growth. (B) Schematic of barcoded evolution experiments and fitness measurement experiments. (C)
272 Table of mutants used in this study, including ploidy, and publication source. (D) Probability density of
273 mutational fitness coefficients. The black line refers to first-step mutants from Levy et al 2015. Colored
274 lines depict the inferred density of fitness effects of mutations from second-step evolution experiments in
275 the 2Day transfer environment (Evo2D). (E) Fitness effects per cycle in 2-Day transfer of all mutants,
276 relative to WT ancestor. First violin plot for each parental strain shows neutral haploids. Second shows
277 pure diploids. Third column is all other 2-Day adaptive mutants, including adaptive haploids and high-
278 fitness diploids. Fourth column is all other 3-Day adaptive mutants. (F) As in (E), but relative to parental
279 strain.

280 **Second-step adaptive clones demonstrate a shift from pleiotropic to modular adaptation**

281
282 Next, to determine whether the pattern of pleiotropic adaptation observed over the first-step of
283 evolution is maintained in the second step, we compared changes in performance for each
284 mutant to its parental strain. To calculate each mutant's performance in fermentation,
285 respiration, and stationary phases, we leveraged differences in each mutant's fitness in
286 experiments of different transfer lengths, which was previously shown to be a good proxy for the
287 direct performance in each growth phase (Y. Li et al. 2018; Y. Li, Petrov, and Sherlock 2019). In
288 particular, a mutant's respiration performance per hour was calculated as the difference
289 between its 2-Day fitness and 1-Day fitness, divided by the 24 hours in respiration phase
290 experienced over the second day (Figure 3A). We then used this respiration performance to
291 extrapolate the mutant's relative fitness at 20 hours, the time at which the population undergoes
292 the diauxic shift from fermentation metabolism to respiration metabolism, with which we can
293 calculate its fermentation performance per hour (Figure 3A). Finally, we calculated a mutant's
294 stationary performance by taking the difference between 5- and 3-Day fitness and dividing it by
295 the 48 hours of stationary phase experienced over these two days (Figure 3A). Importantly, the
296 growth phase performances calculated here reflect compound measurements of several
297 parameters important to fitness during and between growth phases, including energy
298 metabolism, sensing of changing nutrient gradients, and survival.

299
300 We found that while 85% ($\pm 3\%$) of isolated first-step adaptive mutants improved performance in
301 both fermentation and respiration phases (black points within gray square in Figure 3B), only
302 35% ($\pm 1\%$) ($p < 0.001$, re-sampling test) of isolated second step adaptive haploids evolved in the
303 same 2-Day transfer environment improved performance over their first-step parental strain in
304 both phases (light orange points within gray square in Figure 3B). Second-step mutants that
305 were isolated from Evo3D, which encompasses the growth phases of Evo2D, show an even
306 stronger shift from adaptive pleiotropy than the second-step mutants from the Evo2D, with only
307 13% ($\pm 1\%$) of these mutants improving performances in both fermentation and respiration
308 (darker colored points labeled "Evo3D" in Figure 3B, C). This shift is also seen for each parental
309 strain individually (Figure 3C), with Evo2D second-step mutants isolated from each first-step
310 parental strain showing a reduction in the number of mutations that improve performance in
311 both fermentation and respiration, albeit with some variability in magnitude. For example, only
312 25% ($\pm 2\%$) and 17% ($\pm 2\%$) of second-step Evo2D mutants from *IRA1-missense* and *IRA1-*
313 *nonsense* parental strains, respectively, improved both fermentation and respiration
314 performances (Figure 3C). At the same time 51% ($\pm 4\%$), 65% ($\pm 10\%$), and 65% ($\pm 5\%$) of
315 second-step Evo2D mutations improve both fermentation and respiration performances from
316 *CYR1*, *GPB2*, and *TOR1*. Thus while the second step adaptive mutations are still capable of
317 improving fermentation and respiration performances at the same time, the probability of
318 mutations being pleiotropically adaptive is lower.

319
320 In addition to a reduction in the number of second-step mutations that improve performance in
321 both fermentation and respiration phases, we noticed that second-step mutants were much

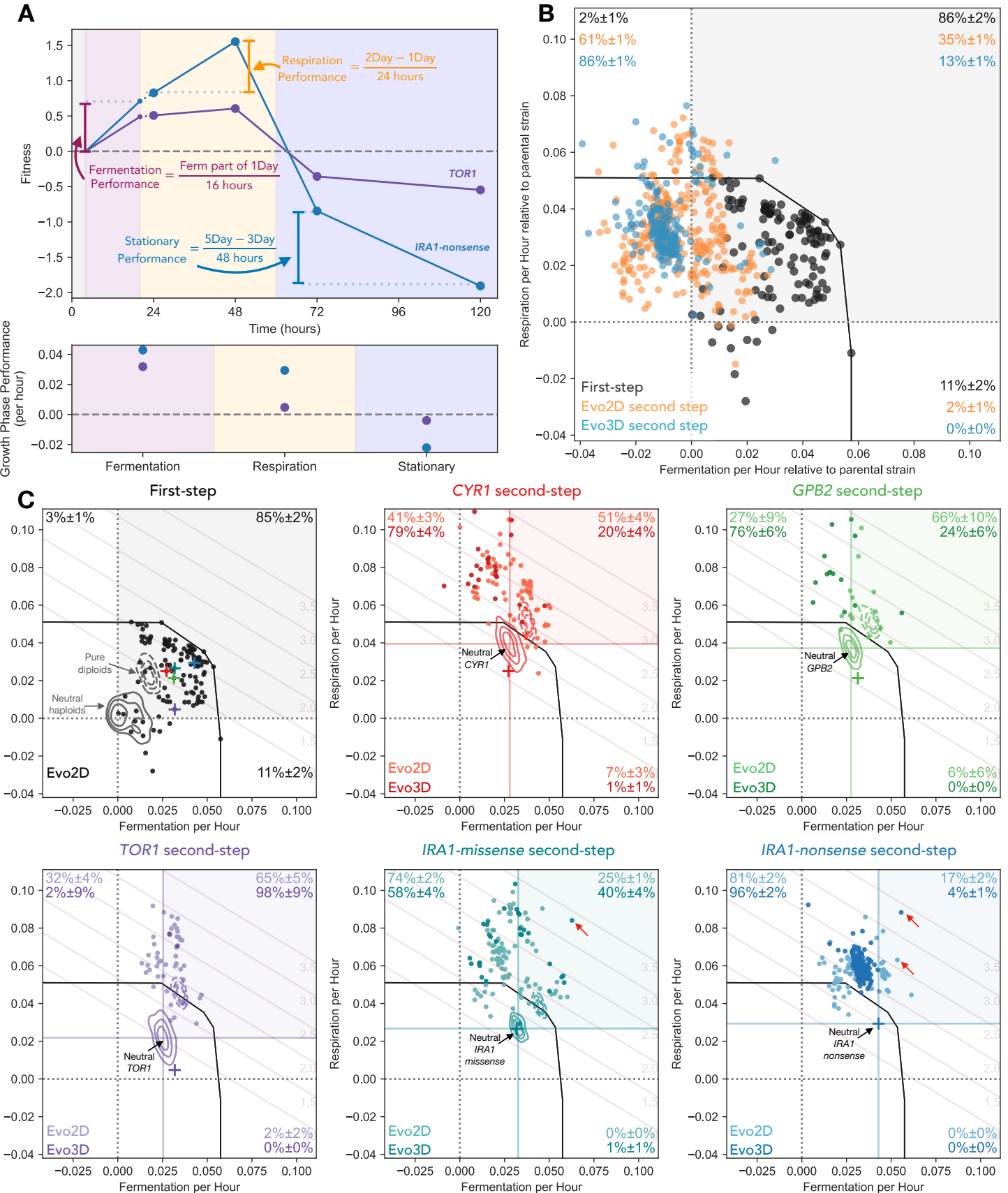
322 more likely to improve respiration performance than fermentation performance. Across all
323 second-step Evo2D mutants, 98% ($\pm 1\%$) improved respiration performance. 61% ($\pm 1\%$) of
324 these mutants improved respiration at the cost to fermentation performance (Figure 3B). This
325 effect is even stronger for Evo3D mutants, where 86% ($\pm 1\%$) improve respiration at a cost to
326 fermentation performance (Figure 3B). This trend holds across most parental strains, with the
327 strongest pattern seen for mutants evolved from the *IRA1-nonsense* parental strain, where 81%
328 ($\pm 2\%$) of Evo2D mutants and 96% ($\pm 2\%$) of Evo3D mutants improved respiration performance
329 at the cost of fermentation performance. Note that while many of these mutants reduce
330 fermentation performance from the initial first-step parental strains, only a small number of
331 mutants have fermentation performances worse than the original ancestor strain (Figure 3C,
332 vertical black dashed line in each subplot).

333

334 At the same time, improving performance in only the fermentation phase is rare. Only 2% of
335 second-step Evo2D mutants and no isolated second-step Evo3D mutants improve fermentation
336 alone, despite the fact that an equivalent improvement in fermentation performance would result
337 in similarly high fitnesses for those mutants in the 2-Day condition these populations were
338 evolved in (see fitness isoclines in Figure 3C).

339

340 Despite these general patterns revealing a shift from pleiotropic to modular adaptation, there are
341 several examples of very strongly adaptive clones which improve both performances. For
342 example, one clone isolated from the *IRA1-missense* population has a fitness advantage of
343 340% per cycle relative to the initial ancestor (or 210% relative to the *IRA1-missense* parental
344 strain). This mutant does improve performance in both fermentation and respiration growth
345 phases, albeit with most of its fitness gain coming from respiration (Figure 3C, *IRA1-missense*
346 panel, labeled with red arrow). We isolated other rare examples of very fit clones that improve
347 both growth phases from other parental strains (Figure 3C, *IRA1-nonsense* panel, labeled with
348 red arrows), suggesting that the yeast have not yet reached functional constraints on the ability
349 to improve both fermentation and respiration performance and that it is still possible to improve
350 both performances beyond the evolutionary constraints observed for the first step of adaptation.
351 As discussed below, some of these very fit clones have acquired third or fourth adaptive steps,
352 allowing them to achieve these high fitnesses.



354 **Figure 3. Second-step adaptive mutants tend to improve respiration performance and not**
355 **fermentation performance.** (A) Performance calculation in each growth phase. Respiration performance
356 (per hour) is calculated as the difference between a mutant's 2-Day and 1-Day fitness, divided by 24
357 hours. To calculate fermentation performance (per hour), we remove four hours of 1-Day fitness that is
358 due to the mutant's respiration benefit. The remaining fitness is then divided by 16 hours of fermentation
359 phase. Stationary phase performance (per hour) is calculated as the difference between 5- and 3-Day
360 fitness divided by 48 hours. Example fitnesses and performances are shown for the *TOR1* and *IRA1-*
361 *nonsense* mutations used as parental strains for the second-step of evolution. (B) Comparison of
362 changes in performances from first- to second-step mutants relative to each parental strain. Note that
363 first-step mutants are shown relative to the initial ancestor (the same as their measured fitness). Second-
364 step mutants are shown relative to the relevant parental strain (i.e. second-step mutants from *IRA1-*
365 *missense* are shown relative to neutral *IRA1-missense* parental lineages). Percentages in corners
366 indicate estimated fraction of mutants in each quadrant as determined by re-sampling of mutants with
367 fitness measurement error. (C) Performance of isolated mutants separated by parental strain. Each
368 mutant's performance in fermentation and respiration growth phases is shown, separated into subfigures
369 by the initial ancestor for each mutant. KDE estimates represent the density of neutral haploids (solid
370 lines) and pure diploids (dashed lines) for each ancestor. Crosses represent the barcoded mutants
371 carrying the first-step mutation from the initial evolution experiment. Black line depicts a convex hull of the
372 most extreme first-step mutants. Fitness isolines show the 2-Day fitness advantage per cycle relative to
373 ancestral strain associated with each location in the performance space.
374

375 **Adaptively modular second-step mutants are more likely to improve performance in**
376 **stationary phase**
377

378 We next asked how the shift from adaptive pleiotropy to adaptive modularity of performances
379 under selection affects how these mutants perform in other tasks not under selection in the
380 Evo2D environment. For example, Li et al (2018) (Y. Li et al. 2018) showed that many of the
381 first-step mutations, which tended to improve both fermentation and respiration performances,
382 exhibited costs in stationary phase performance. Does the shift towards adaptive modularity
383 reduce the likelihood or magnitude of costs in other performances, potentially indicating that
384 these mutants are more modular overall? Or do these costs to other performances remain?
385

386 To address these questions, we calculated each mutant's performance in stationary phase
387 (Figure 2A). As previously described (Y. Li et al. 2018), first-step mutants are more likely to
388 incur a cost in stationary phase than to improve it (Figure 4A), with 30% (36/119) of mutants
389 showing such a cost (Figure 4B) and less than 2% (2/119) showing any improvement in
390 stationary performance. The most fit first-step mutants which improve both fermentation and
391 respiration performance to substantial degrees tend to have larger costs in the stationary phase.
392 In particular, the *IRA1-nonsense* mutants, which were the most fit in the first-step, have the
393 strongest costs in stationary phase performance, up to -4% per hour (Figure 4A).
394

395 We find that many Evo2D second-step mutants do pay a cost in stationary phase. In particular,
396 42% of second-step Evo2D adaptive mutants have lower stationary performance than their
397 parental strain. At the same time, these costs to stationary performance tend to be somewhat

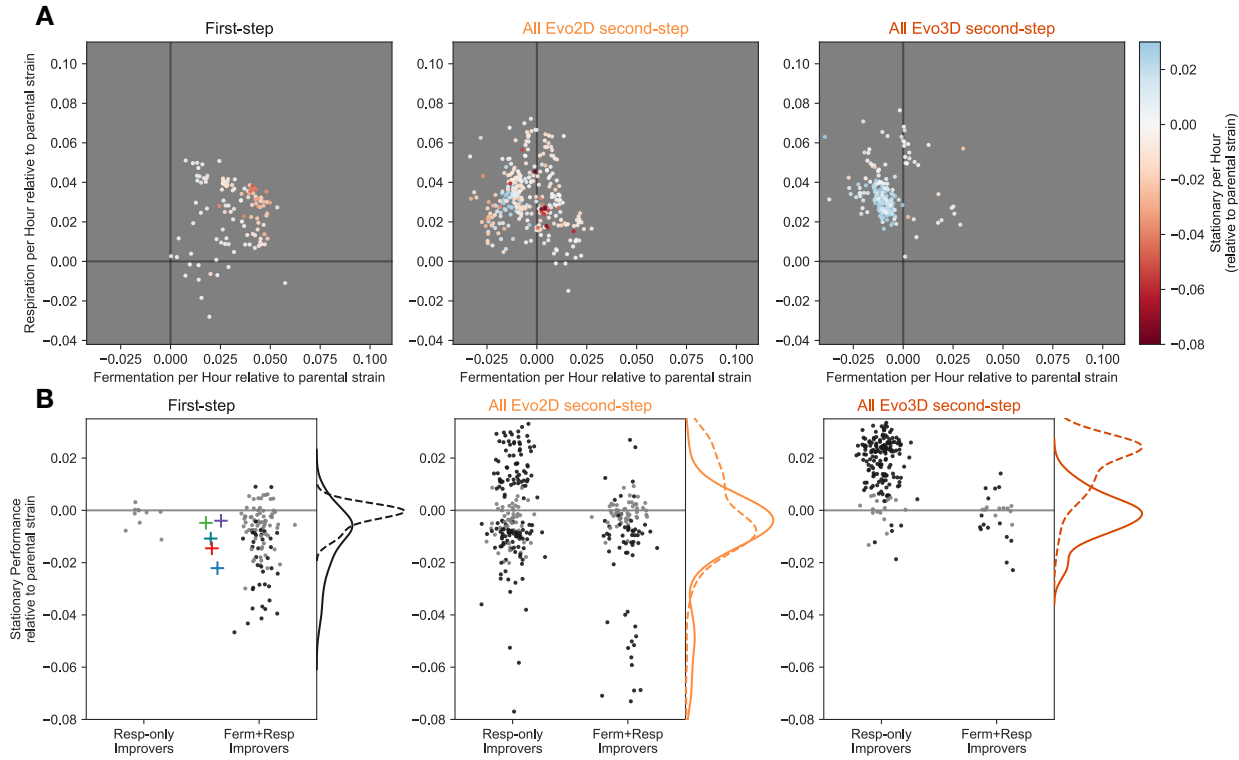
398 minor, exhibiting costs of less than -2% per hour for second-step mutants derived from *CYR1*,
399 *GPB2*, *TOR1*, or *IRA1*-missense parental strains (Figure 4B). Note that this was not the case for
400 the second-step mutants isolated from *IRA1*-nonsense populations, which exhibited the
401 strongest costs to stationary phase in the first-step of evolution. These second-step mutants had
402 further costs to stationary performance as extreme as -10% per hour (see supplemental figures
403 S3 and S4).

404

405 However, in contrast to the first-step of evolution where stationary performance was rarely
406 improved, 25% (77/306) of second-step Evo2D mutants show an increase in stationary
407 performance (Figure 4A). We further stratified the second-step mutants based on their
408 combined fermentation and respiration performances. Specifically, we asked whether mutants
409 that only improve respiration performance showed behavior in stationary phase that was distinct
410 from those that improved both fermentation and respiration performance. We find that second-
411 step Evo2D mutants that only improved respiration performance had varied effects on stationary
412 performance, with 36% (70/197) showing increased stationary performance and 39% (76/197)
413 showing a cost to stationary performance. By contrast, second-step Evo2D mutants that
414 improved both fermentation and respiration performances were much less likely to improve
415 stationary performance, with only 6% (7/109; $p < 1e-8$ compared to by respiration-only improvers
416 by Fisher's exact test) of these mutants showing stationary improvement and 49% (53/109)
417 imposing a cost on yeast's ability to survive stationary phase.

418

419 Thus, it appears that mutations that are capable of improving both fermentation and respiration
420 at the same time are more likely to incur costs in stationary phase. This inherent relationship
421 may explain the reduction in Evo3D mutants that improve both fermentation and respiration
422 performances (Figure 3B, 4A), as stationary phase is additionally under selection in this
423 condition. Indeed, 79% (160/202; $p < 1e-8$ compared to Evo2D by Fisher's exact test) of Evo3D
424 mutants show an improvement in stationary phase, 97% (155/160) of which do not improve
425 fermentation. While 7% (15/202) of Evo3D mutants do exhibit a cost in stationary phase, these
426 costs are relatively minor and are primarily found in mutants with combined fermentation and
427 respiration performances that compensate for these costs to stationary performance (Figure 4A
428 and B). These data indicate that the shift from mutants that improve both fermentation and
429 respiration performances to those that primarily improve respiration performance is
430 accompanied by a change in stationary phase performance. This pattern is true even when the
431 other performance (stationary phase) is not under selection, as is in the case of Evo2D,
432 suggesting that the pleiotropic "side effects" - that is phenotypic effects of mutations that are not
433 primarily under selection (Kinsler, Geiler-Samerotte, and Petrov 2020) - of these second-step
434 mutants may differ more generally from those of the first-step mutants.



435
 436 **Figure 4. Mutations that improve respiration performance only exhibit less extreme costs in stationary phase**
 437 **compared to those that improve fermentation and respiration performances.** (A) Each panel depicts mutant
 438 performance relative to their parental strain, colored by the relative stationary phase performance of the parental
 439 strain (see color bar). The first panel shows all first-step mutants. The second and third panels depict second-step
 440 mutants isolated from Evo2D and Evo3D conditions, respectively. (B) Each panel shows the stationary performance
 441 relative to the mutants' respective parental strains. Mutants are split according to the effect on fermentation and
 442 respiration performances. Those which improve both fermentation and respiration are categorized as "Ferm+Resp
 443 Improvers" and all other mutants are categorized as "Resp-only improvers". Black points represent those with
 444 measurement error that does not overlap 0. Gray points have measurement error that show no significant change in
 445 stationary performance relative to the parental strain. Panels are organized as in (A). Kernel density estimates show
 446 the relative density for respiration-only improvers (dashed line) and fermentation and respiration-improving mutants
 447 (solid line).

448
 449 **Changes in selection pressure and physiological limitations do not explain the shift**
 450 **towards modular adaptation**

451
 452 Thus far, we have shown that there is a general shift in the effect that adaptive mutations have
 453 on performance in growth phases over the course of a two-step adaptive walk. In particular, we
 454 find that while first-step mutations exhibit adaptive pleiotropy, improving both fermentation and
 455 respiration performances, second-step mutations isolated from the same Evo2D environment
 456 tend to be adaptively modular, improving only respiration performance and often at the cost to
 457 fermentation performance. What could be driving this shift? There are three primary possibilities
 458 for this observation. One possibility is that, while care was taken to ensure the evolution
 459 condition was as consistent as possible to the first step of evolution, the selection pressure in

460 the second-step evolution experiments was shifted to favor respiration performance more than
461 fermentation performance. A second possibility is that the populations have reached
462 physiological limits on the yeast's ability to ferment glucose, such that there is more room to
463 improve respiration performance. Finally, it could be that genetic and signaling pathways are
464 wired such that there are only a limited number of mutational targets available to further improve
465 both fermentation and respiration performances in the second-step of evolution.
466

467 The first possible explanation for the shift towards modular adaptation is that the second-step of
468 evolution was accompanied by a change in the relative contribution of fermentation and
469 respiration growth phases to fitness in the 2-Day transfer condition. While we took care to
470 ensure that the population sizes, transfer times, media conditions, and other details were
471 identical to the conditions used in the first-step evolution experiment, it could be possible that
472 differences remain. For example, the identity of the strain comprising the majority of the
473 population in second-step evolution experiments may have shifted the selection pressures to
474 increase the importance of respiration performance compared to the first step of evolution. To
475 test whether there was such a shift, we compared the fitness effects of mutations in the
476 evolution experiment itself with our fitness measurement experiments, which more closely mimic
477 the first-step evolution experiments because the ancestral strain comprises the majority of the
478 population. Specifically, we calculated the partial correlation between respiration performance
479 and fitness during the evolution experiment, accounting for the fitness inferred from our fitness
480 measurement experiments. If respiration performance contributes more to evolution fitness than
481 expected from our fitness measurement experiments, we would expect a positive partial
482 correlation after this adjustment. However, this is not the case ($r=-0.02$, $p=0.74$), indicating that
483 the shift from pleiotropic to modular adaptation is not due to a change in selection pressure (see
484 Methods, Differences in selection pressure do not drive shift towards modular adaptation).
485

486 The second possible explanation for the shift towards modular adaptation is that the yeast have
487 reached physiological limits on the ability to improve fermentation performance. To test whether
488 yeast have reached the upper limits of fermentation performance, we performed additional
489 evolution experiments in a 1-Day transfer environment, which primarily selects for fermentation
490 performance. From these experiments, we isolated at least one second-step mutation from the
491 *IRA1*-nonsense population that improved fermentation performance above the highest
492 fermentation performances achieved by first- or second-step mutations evolved in the 2-Day
493 and 3-Day environments (see Fig S2). This suggests that while a fermentation performance
494 maximum has not yet been reached, the pre-existing wiring of genetic and signaling pathways
495 may be such that it is much easier to find mutations that improve respiration performance at the
496 cost of fermentation performance than it is to find mutations that improve both fermentation and
497 respiration performances or even fermentation performance at the cost to respiration
498 performance.

499 **Second step adaptive mutations reveal a shift from mutational targets in general nutrient-**
500 **sensing pathways to specific processes involved in mitochondrial function**

501
502 To better understand these patterns of pleiotropy and to identify the genetic basis of adaptation
503 in these environments, we performed whole-genome sequencing on 324 adaptive mutants and
504 called variants (see Methods). To identify the likely adaptive mutations, we compared the genes
505 across all isolated mutants from all evolution experiments and labeled genes that were hit more
506 than three times across all mutants as putatively causal. After identifying pathways that were
507 recurrently targeted, we further identified genes belonging to the same pathways and called
508 these as putatively causal as well.

509
510 From this whole-genome sequencing, we found some adaptive targets in nutrient-sensing
511 pathways that were previously identified in the first-step of evolution. The first-step of adaptation
512 typically involved mutations in one of two signaling pathways responsible for sensing glucose
513 and instructing the cells to grow: the Ras/PKA and TOR/Sch9 pathway (Venkataram et al.
514 2016), Table 1). Most of these mutations resulted in loss of function in negative regulators of the
515 pathway or modification of function in positive regulators, ultimately driving constitutive
516 activation of these pathways (Venkataram et al. 2016). In an analysis of the second-step of
517 evolution for *TOR1*, *CYR1*, and *GPB2* mutants in the 2-Day environment, Aggeli et al (2021)
518 identified Ras/PKA pathway mutations as an adaptive route for *TOR1* mutants and TOR/Sch9
519 mutants as an adaptive route for *CYR1* and *GPB2* mutants. The additional sampling we've
520 conducted here, including sequencing mutants isolated from the two *IRA1* populations under
521 Evo2D and Evo3D, further confirm that TOR/Sch9 pathway mutations are commonly observed
522 in the background of Ras/PKA mutants. In particular, we find that mutations in the gene *KSP1*, a
523 PKA-activated kinase which inhibits autophagy via TORC1 (Umekawa and Klionsky 2012;
524 Chang and Huh 2018), are common across all of the Ras/PKA parental strains (Table 1). These
525 mutations were most commonly isolated from *IRA1*-nonsense populations, where 42% (32/77)
526 of Evo2D mutants and 91% (30/33) of Evo3D mutants harbored a *KSP1* mutant. Unlike the
527 TOR/Sch9 pathway mutants observed in the first-step of evolution, which putatively result in
528 increased TORC1 activity, increased cell growth, and decreased autophagy (Wilson and Roach
529 2002; Venkataram et al. 2016), many of the observed second-step *KSP1* mutations are loss-of-
530 function . This indicates that these mutations may be acting in the opposite direction of first-step
531 mutations in this pathway, potentially allowing for the up-regulation of TOR despite (or in
532 compensation of) increased activation of PKA associated with the Ras/PKA mutants.

533
534 Beyond mutations in nutrient-sensing signaling pathways commonly being observed in the first-
535 step of adaptation, our sampling reveals a shift towards mutational targets related to
536 mitochondrial function and respiration, which likely affect the respiration performance of mutants
537 measured in our study (Table 1). In particular, we find that 36% (22/64) of adaptive mutants
538 isolated from *IRA1*-missense populations in the 2-Day evolution condition acquire mutations in
539 or near genes involved in the TCA cycle (*CIT1*, *KGD1*, *MDH1*, *MAE1*, *ALD5*). Interestingly, all of
540 these mutations are either missense or putatively regulatory mutations in enzymes directly

541 responsible for respiration, suggesting they may modify the function or expression of these
542 enzymes, potentially changing respiratory flux (Suissa, Suda, and Schatz 1984; Kurita and
543 Nishida 1999; Navarro-Aviño et al. 1999; Repetto and Tzagoloff 1989; Ait-EI-Mkadem et al.
544 2017; Reinders et al. 2007; McAlister-Henn and Thompson 1987; Boles Eckhard, de Jong-
545 Gubbels Patricia, and Pronk Jack T. 1998). In addition, we identified mutations in several genes
546 related to the regulation of respiration and mitochondrial function, with 25% (16/64) of isolated
547 2-Day *IRA1*-missense mutants identified as carrying a mutation in the RTG pathway, which is
548 responsible for the regulation of genes important for respiration. In particular, we observe
549 putative loss-of-function mutations in *MKS1*, a negative regulator of the RTG pathway, and
550 missense mutations in *RTG2*, a positive regulator of the pathway (Liu et al. 2003; Liao and
551 Butow 1993; Komeili et al. 2000; T. Sekito, Thornton, and Butow 2000; Takayuki Sekito et al.
552 2002). This suggests that these mutations may be up-regulating the RTG pathway and the
553 genes it regulates, indirectly increasing metabolic flux through the TCA cycle. Moreover, 19%
554 (12/64) of these mutants carry a mutation in other genes related to the regulation of
555 mitochondrial biogenesis (*PUF3*, *PAB1*, *PAN1*, *PAN2*, *AIM17*), many of which are related to
556 post-transcriptional modification of mRNA molecules related to mitochondrial function or
557 respiration (Chaithanya and Sinha 2023; C.-D. Lee and Tu 2015; Lapointe et al. 2018).

558

559 These patterns are also observed in other populations harboring different first-step mutants. In
560 particular, while our sampling for *IRA1-nonsense* and *IRA1-missense* populations allowed us to
561 detect the largest number of mutational targets, mutations in genes involved in the TCA cycle,
562 RTG pathway, and mitochondrial biogenesis were found in populations from nearly all first-step
563 mutations, with a few exceptions. These exceptions, for example the absence of HOG-pathway
564 mutations from *IRA1-missense* and *IRA1-nonsense* backgrounds, is suggestive of historical
565 contingency, where the identity of further mutations is dependent on mutations acquired earlier
566 in evolution (Blount, Borland, and Lenski 2008; Harms and Thornton 2014; Park, Metzger, and
567 Thornton 2022; Bakerlee et al. 2021). While some of these genes were detected in previous
568 work (Aggeli, Li, and Sherlock 2021), additional sampling from new evolution experiments in the
569 3-Day condition and additional parental strains (*IRA1-missense* and *IRA1-nonsense*) allowed us
570 to more confidently identify recurrently mutated genes and to group the observed sets of
571 mutations and genes into functional categories and pathways.

572

573 **Mutations isolated from the 3-Day evolution experiment are a subset of 2-Day adaptive 574 mutants**

575

576 We next examined whether there was a difference in the mutational targets isolated from 2- and
577 3-Day evolution experiments, given that we observed that Evo2D mutants were more likely to
578 improve both fermentation and respiration performances than Evo3D mutants (Figure 3), and
579 Evo3D mutants were more likely to improve stationary performance than Evo2D (Figure 4). In
580 particular, we wondered whether the addition of stationary phase as a selective pressure
581 allowed for new mutational targets to be adaptive because of their effect on stationary phase, or

582 if instead, the addition of stationary phase restricted the Evo3D mutational targets to a subset of
583 the Evo2D mutations that were not costly to stationary performance.

584

585 By comparing the sets of mutated genes for well-sampled parental strains *IRA1-missense* and
586 *IRA1-nonsense*, we saw that all genes mutated in the 3-Day evolution experiments were also
587 identified in the 2-Day evolution experiments (see Table 1). In particular, *PUF3*, *PAB1*, and
588 *MTH1* mutants are entirely absent as single mutations from the 3-Day *IRA1-nonsense*
589 experiments, shifting the molecular targets to essentially just those in *KSP1*. Similarly, RTG and
590 TCA cycle mutants are reduced in frequency or absent from the 3-Day *IRA1-missense*
591 experiments, respectively. As expected, these mutations that are reduced in frequency show
592 costs in stationary performance and thus have reduced fitness in the 3-Day transfer
593 environment (Figs S7 and S8).

	WT	<i>TOR1</i>	<i>GPB2</i>	<i>CYR1</i>	<i>IRA1-missense</i>	<i>IRA1-nonsense</i>				
	Evo2D	Evo2D	Evo3D	Evo2D	Evo3D	Evo2D	Evo3D	Evo2D	Evo3D	
Ras/PKA Pathway	<i>IRA1</i>	30/77					1/30*			Loss of function
	<i>IRA2</i>	11/77	1/21							Loss of function
	<i>GPB1</i>	4/77		1/7*						Modification of function
	<i>GPB2</i>	14/77	2/21							Loss of function
	<i>PDE2</i>	11/77								Modification of function
	<i>CYR1</i>	3/77								Modification of function
	<i>GPR1</i>				1/27					Modification of function
	<i>RAS2</i>	1/77	1/21							Modification of function
TOR/Sch9 Pathway	<i>TFS1</i>	1/77								Modification of function
	<i>TOR1</i>	1/77								Modification of function
	<i>KOG1</i>	1/77								Modification of function
	<i>SCH9</i>			1/7						Modification of function
HOG Pathway	<i>KSP1</i>			1/7	1/8*	1/27	2/14	4/67		32/72 30/33
	<i>HOG1</i>					1/27				Loss of function
	<i>PBS2</i>		6/21							Modification of function
	<i>SSK2</i>		7/21		1/7	1/8	1/27			Modification of function
RTG Pathway	<i>RTG2</i>				1/8	4/27	2/14	9/67	1/30	1/72
	<i>MKS1</i>					2/27	1/14	7/67	1/30*	Loss of function
	<i>BMH1</i>			1/7*		1/27				Modification of function
	<i>CIT1</i>		1/21			1/27		16/67	1/30	Modification of function
TCA cycle	<i>KGD1</i>					1/27		3/67		Modification of function
	<i>MDH1</i>							4/67		Modification of function
	<i>MAE1</i>							2/67		Modification of function
	<i>ALD5</i>					1/14		1/67*		2/72*
Regulation of Mitochondrial Biogenesis	<i>PAB1</i>		1/21		2/8	1/27	4/14	3/67	5/30	12/72
	<i>PAN2</i>							2/67		Modification of function
	<i>PAN3</i>		1/21					1/67		Modification of function
	<i>AIM17</i>				1/8			2/67		Loss of function
Other	<i>PUF3</i>				1/8	4/27	2/14	7/67	7/30	24/72 1/33*
	<i>MKT1</i>			1/7	1/8	1/27	1/14	1/67	9/30	Modification of function
	<i>GSH1</i>		1/21		1/7	5/27		2/67	1/30	Modification of function
	<i>ARO80</i>					3/27	1/14	3/67	4/30	Loss of function

594 **Table 1. Identified mutations by ancestral genotype and evolution condition.** Boxes with gray text
595 and asterisks indicate genes mutated only in the context of other putatively causal mutants. The column
596 on the far right indicates the putative functional effect of the mutations on the gene. If any stop-gained or
597 frameshift mutations were identified in this gene, it was classified as harboring “loss of function”
598 mutations. If instead, only missense or nearby non-genic mutations were identified, the gene is classified
599 as “modification of function”.

600 **The exhaustion of mutational targets in nutrient-sensing signaling pathways drives the**
601 **shift towards modular adaptation**

602
603 To understand how the shift from pleiotropic to modular adaptation over the two-step adaptive
604 walk is reflected on a molecular basis, we examined how each of these mutations moved the
605 organisms in the performance space. The first step of evolution, which primarily hit mutational
606 targets in the Ras/PKA pathway, shows strong patterns of pleiotropic adaptation, with these
607 mutations improving both fermentation and respiration performances (Figure 5A).

608
609 Of the second-step adaptive haploids, those with mutations in the Ras/PKA pathway (Figure 5B,
610 blue circles), which were isolated primarily from the *TOR1* populations, also display pleiotropic
611 adaptation, improving both fermentation and respiration performance. This suggests that
612 mutations which putatively increase the activity of the Ras/PKA pathway are indeed generally
613 adaptively pleiotropic.

614
615 In addition to Ras/PKA mutations, other haploids with mutations in *ARO80* (Figure 5B, pink
616 circles) and *GSH1* (Figure 5B, gold circles), show recurrent patterns of pleiotropic adaptation
617 across parental strains, notably across *CYR1* and *IRA1*-missense genetic backgrounds (Figures
618 S5 and S6). Mutations in these genes, which are involved in amino acid catabolism (Iraqui et al.
619 1999; K. Lee and Hahn 2013) and glutathione biosynthesis (Kistler, Maier, and Eckardt-Schupp
620 1990), respectively, may be adaptively pleiotropic due to their involvement in processes entirely
621 orthogonal to, or upstream of, both fermentation and respiration.

622
623 Many of the remaining mutational targets improve respiration performance at the cost of
624 fermentation performance. In particular, haploid mutants which harbor mutations in genes
625 involved in the TCA cycle (Figure 5B, green circles), mitochondrial biogenesis (orange, red
626 circles), or the RTG pathway (brown circles) improve respiration performance at the cost to
627 fermentation performance in *CYR1*, *GPB2*, *TOR1*, and *IRA1*-missense backgrounds when
628 present (Figure 5). Notably, haploids that harbor mutations in these genes have similar fitness in
629 the 2-Day transfer environment to mutants with mutations in *ARO80* and *GSH1*, which exhibit
630 adaptive pleiotropy. Despite these similar fitnesses, there is an 8-fold increase in observed
631 adaptively modular genetic targets than those that are adaptively pleiotropic in the *IRA1*-
632 missense 2-Day evolution experiments (41 mutants in TCA and RTG with fitnesses between 2.0
633 and 2.5 compared to 5 in *GSH1* and *ARO80* for *IRA1*-missense).

634
635 There are also single point mutations in *MKT1* which achieve very high 2-Day fitness by greatly
636 improving respiration performance and showing little cost to fermentation performance (Figure
637 5B - chartreuse circles). Interestingly, all adaptive mutations in this gene occur at the same
638 nucleotide, changing from 89A to C, G, or T. Thus, while these mutations are driven by only a
639 single mutation, their lower frequency reflects the reduced target size compared to the other
640 haploid mutations which have multiple targets within the gene (e.g., those in RTG pathway, TCA
641 cycle, etc.). The 89A allele is a derived allele in the parental S288C yeast strain used for all of

642 these experiments and reflects an ancestral reversion in the case of A89G. This A89G reversion
643 has been previously observed in other evolution experiments in glucose limitation and the 89G
644 allele has been shown to stabilize mRNA of mitochondrial genes that are targets of Puf3
645 (Chaithanya and Sinha 2023; Gupta et al. 2015). Interestingly, 89C and 89T alleles each
646 provide similar fitness benefits as the 89G allele in our experiments despite resulting in distinct
647 amino acids, suggesting that the 89A allele and the resulting aspartic acid may be particularly
648 costly to *MKT1* function.

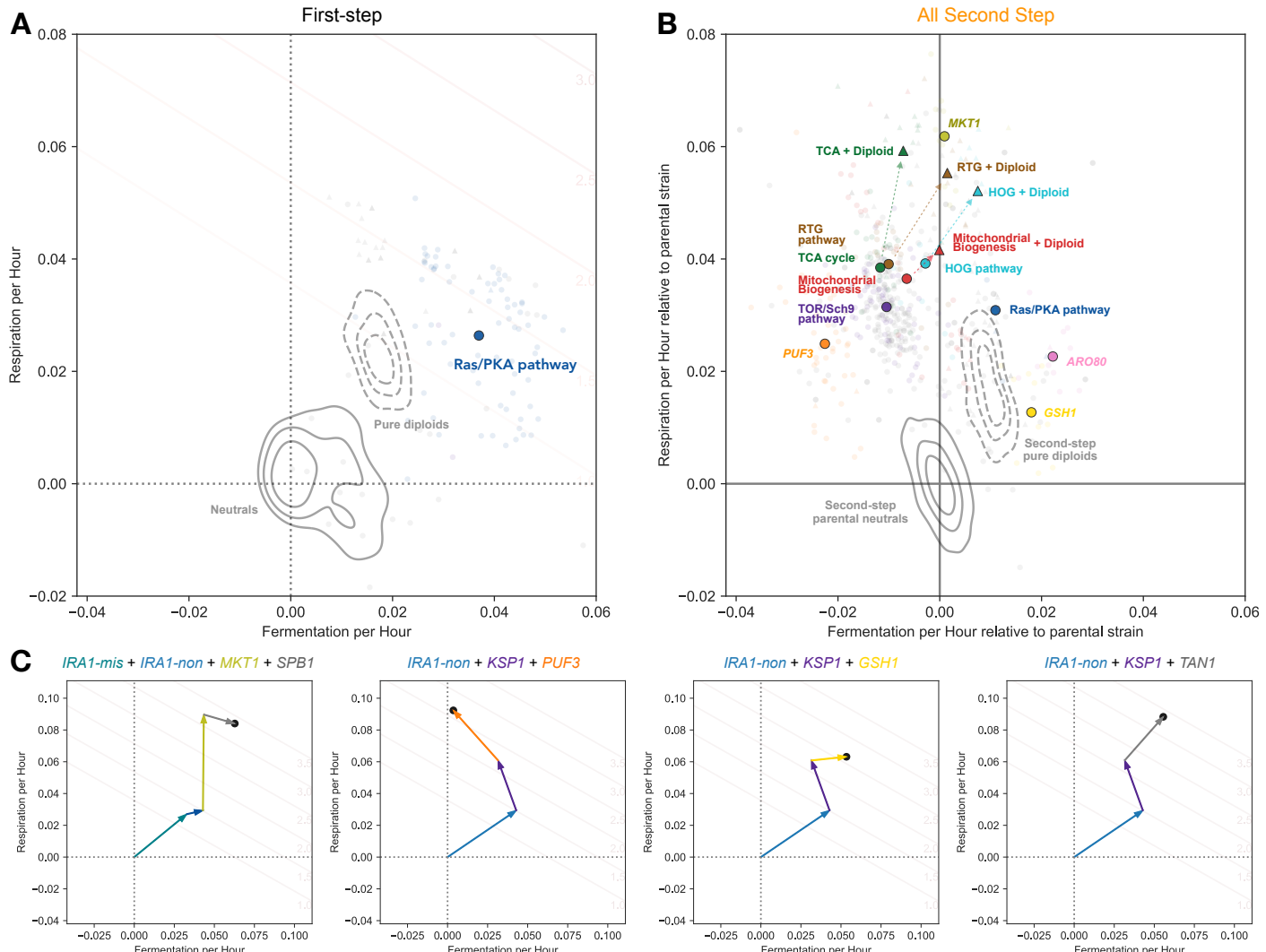
649

650 Beyond adaptive mutations in haploids, auto-diploidization is a common mode of adaptation. In
651 particular, we see that in addition to diploidy being adaptively pleiotropic by itself (pure diploids
652 shown as topographical Kernel Density Estimates in Figure 5), high-fitness diploids that co-
653 occur with other mutations (colored triangles in Figure 5) also show patterns of adaptive
654 pleiotropy, improving both fermentation and respiration performances. This seemingly universal
655 benefit without cost likely explains the high frequency of auto-diploidization observed across
656 genetic backgrounds and environmental conditions in many yeast evolution experiments (Tung
657 et al. 2021; Venkataram et al. 2016; Levy et al. 2015; Hong and Gresham 2014; Fisher et al.
658 2018). While these high-fitness diploids provide a much larger benefit than haploids that harbor
659 mutations in the same genes, their reduced frequency is likely due to a lower mutation rate, as
660 these mutants needed to acquire both a mutation in an adaptive target and auto-diploidize,
661 together improving respiration to a larger extent and mostly eliminating costs to fermentation
662 performance associated with the mutation. Notably, most of the point mutations are
663 homozygous, indicating they likely occurred before the auto-diploidization event.

664

665 In addition to these general trends, we sampled a small number of mutations that have a total of
666 three or four putatively causal mutations since the original ancestor. These mutants provide
667 hints about how adaptation might proceed over longer adaptive walks. In one case, as
668 demonstrated by the *IRA1*-nonsense + *KSP1* + *PUF3* mutant depicted in the second panel of
669 Figure 5C, we observe adaptation as continuing down a route towards specialization in
670 respiration performance. We also observe three examples where the collective effect of the
671 mutations instead drives evolution towards generalism – improving both fermentation and
672 respiration performance – despite being composed of second-, third-, and fourth-step mutations
673 which tend to improve only one performance or the other. For instance, one *IRA1*-missense
674 mutant acquired an *IRA1*-nonsense mutation, an *MKT1* A89G mutation which improves only
675 respiration by itself in this background, and acquired a mutation in *SPB1* (Suppressor of *PAB1*),
676 which is expected to improve only fermentation with a modest cost to respiration, assuming
677 additive mutational effects in the performance space (Figure 5C, first panel). We see similar
678 examples for two *IRA1*-nonsense mutants: one of which acquired both *KSP1* and *GSH1*
679 mutations and the other of which acquired *KSP1* and *TAN1* mutations (Figure 5C, third and
680 fourth panels), where the collective effects of the observed mutations ultimately continue to
681 push the population towards improving both traits. These rare mutants demonstrate that, at
682 least on short evolutionary timescales, navigation of the performance space seems to be more
683 driven by constraints imposed by the genetic wiring of the cell, which influences the relative

684 ease of improving one performance or the other, rather than fundamental or physiological
 685 constraints upon improving the performances themselves.
 686



687 **Figure 5. Adaptive modularity is driven by the accessibility of mutational targets that improve**
 688 **respiration at the cost of fermentation. (A)** Ras/PKA and TOR/Sch9 mutants from the first-step of
 689 adaptation to improve both fermentation and respiration performance. **(B)** Most common second-step
 690 mutational targets tend to improve respiration at the cost of fermentation (centroids depicted as colored
 691 circles), except for rare Ras/PKA (blue), ARO80 (pink), or GSH1 (yellow) mutants; haploids shown as
 692 circles. Auto-diploids exhibit adaptive pleiotropy (dashed KDE estimate for all parental strains, colored by
 693 first-step mutation). Auto-diploidization is also adaptively pleiotropic on the background of other point
 694 mutations (triangles colored by pathway or gene category). Note that only centroids for each category of
 695 gene with at least 3 observed mutants were included. **(C)** Triple and quadruple mutants can ultimately
 696 drive adaptation towards adaptive pleiotropy (or adaptive modularity) despite being primarily composed of
 697 adaptively modular mutations. Note that the mutations beyond the first step are depicted in no particular
 698 order in these subpanels.

699 **DISCUSSION**

700

701 In this study, we sought to understand the frequent observation that single adaptive mutations
702 observed in experimental evolution, especially those of large effect, can pleiotropically improve
703 multiple distinct performances at once. This observation is puzzling because theoretical work
704 suggests that as pleiotropy increases, large effect adaptive mutations should become less
705 probable. This expected “cost of complexity” is the reason for why modularity is often seen as
706 the necessary condition and the expected consequence of evolution of complex organisms by
707 natural selection (Orr 2000; Welch and Waxman 2003; Wagner and Zhang 2011; Wagner,
708 Pavlicev, and Cheverud 2007; Wagner and Altenberg 1996; Melo et al. 2016; Hartwell et al.
709 1999).

710

711 We focused on one striking example of pleiotropic adaptation that comes from previous studies
712 of yeast evolving in a glucose-limited environment (Levy et al. 2015) in which 85% of the first-
713 step single adaptive mutations improved performance in both fermentation and respiration
714 growth phases (Fig1A, Fig3B) (Levy et al. 2015; Venkataram et al. 2016; Y. Li et al. 2018),
715 despite these growth phases as being thought to be physiologically distinct.

716

717 Here, we investigated whether adaptation in the same low-glucose environment and 2-Day
718 transfer as the original experiment (Levy et al. 2015) will continue following the path of adaptive
719 pleiotropy (Fig. 1B) or will shift to become more modular (Fig. 1C). We thus further evolved 5
720 different first-step mutants, four in the Ras/PKA pathway (*IRA1-nonsense*, *IRA1-missense*,
721 *CYR1*, and *GPB2*) and one in the Tor/Sch9 pathway (*TOR1*), sampled a large number of
722 adaptive mutants, and evaluated their effects on the fermentation and respiration performances.
723

724 In all five cases, the results were qualitatively similar. First, adaptation proceeded to improve
725 fitness, albeit to a somewhat muted degree. Second, while a number of mutants were adaptively
726 pleiotropic, improving both fermentation and respiration performances, the dominant trend
727 switched towards more modular adaptation. Specifically, nearly all adaptive mutants improved
728 respiration performance sharply and many had no or only weakly positive or even negative
729 effects on the fermentation performance (Fig. 3B). These results support a model of adaptation
730 wherein early adaptation is driven by mutations of large effect that improve multiple
731 performances at once. Then, after these mutations have become exhausted, adaptation may
732 proceed via more modest mutations that improve performances in a stepwise manner (Figure
733 1C).

734

735 One remaining question is how pleiotropic adaptation is possible in the first place. The
736 prevalence of the pleiotropic adaptation in the first step may be due to these mutations being
737 primarily in Ras/PKA pathway genes. We thus hypothesized that the adaptive pleiotropy is a
738 consequence of the way this pathway has evolved to shift rates of metabolism in both
739 fermentation and respiration in a substantial, coordinated, and beneficial fashion (Wilson and
740 Roach 2002). The notion is that even though these metabolic functions are distinct, they are

741 often required to be carried out in tandem, as respiration commonly follows fermentation for
742 yeast. It is possible that sensing and signaling pathways such as the Ras/PKA pathway evolved
743 to affect them together. This might be a general feature of signaling pathways as they must shift
744 multiple functions and performances together and this ability then represents an attractive target
745 for adaptive genetic changes.

746

747 If pleiotropic adaptation is a feature of the Ras/PKA pathway, the prediction is that 2nd step
748 adaptive Ras/PKA pathway mutations will remain adaptively pleiotropic. This is indeed the case.
749 Second-step mutations in the Ras/PKA pathway, mainly arising in the *TOR1* background, do
750 improve both fermentation and respiration performances. A small number of second-step
751 adaptive mutations outside of this pathway, in *ARO80* and *GSH1*, are also pleiotropically
752 adaptive and improve both respiration and fermentation, but to a smaller degree than Ras/PKA
753 pathway mutants. This suggests that the Ras/PKA pathway is virtually unique in its ability to
754 modulate both fermentation and respiration performances together to a substantial degree in an
755 adaptive manner, a notion also supported by the fact that we observe the shift towards
756 modularity adaptation already in the second adaptive step.

757

758 A small number of adaptive clones in the second step improved both fermentation and
759 respiration performances to a substantial degree. Sequencing of these clones showed that they
760 acquired multiple mutations, and several of these clones improved both performances by the
761 addition of two or more orthogonal steps. This suggests that adaptation can continue improving
762 both performances but the adaptive walk needs to engage multiple modules and multiple
763 mutations, making such adaptation slower than the first step of adaptation. This might be part of
764 the reason why adaptation in general slows down over the course of evolution (Wiser, Ribeck,
765 and Lenski 2013; Johnson et al. 2021; Good and Desai 2015; Aggeli, Li, and Sherlock 2021).

766

767 We argue that signaling pathways such as Ras/PKA have the capacity of generating “coherent
768 pleiotropy”, where the output of many cellular processes can be affected without disrupting the
769 proper regulation and function of each process. As such, signaling pathways that have been
770 evolutionarily pre-wired to control combinations of selective pressures may be easily modified
771 by mutation to coherently improve the performances under selection. The ability of signaling
772 pathways to generate coherent pleiotropy implies that many adaptive mutations should hit
773 signaling pathways. Indeed, this is what we see. For example, in cancer, the key oncogenes are
774 located along cellular signaling pathways and engage either receptors of signals or represent
775 key relay stations in these pathways (Bailey et al. 2018; Sanchez-Vega et al. 2018; Pawson and
776 Warner 2007; Sondka et al. 2018; Hanahan and Weinberg 2011; Hanahan 2022).

777

778 On the other hand, this coherent pleiotropy of signaling pathways does not necessarily indicate
779 that such mutations have no costs in other traits. Indeed, we see that many of the Ras/PKA
780 mutants exhibit costs in stationary phase. Moreover, in previous work, we find that the Ras/PKA
781 mutants have additional phenotypic effects with minor contributions to fitness in the Evo2D
782 evolution condition but substantial effects in other conditions (Kinsler, Geiler-Samerotte, and

783 Petrov 2020). Thus, we might expect these signaling pathways to be most likely to be targeted
784 by adaptation in relatively simple environments where the beneficial pleiotropic effects can be
785 realized with only minor other costs.

786

787 In addition to cellular signaling pathways, other gene-regulatory, hormonal, and neuronal
788 systems allow for organisms to be phenotypically plastic and involve coherent control of many
789 traits of an organism. As such, these systems may also be attractive targets for evolutionary
790 change, as they can serve as high-leverage routes for altering many traits simultaneously. The
791 evolution of phenotypic plasticity hence paves the way for subsequent large-effect evolutionary
792 shifts in local adaptation.

793

794 Finally, we believe that the existence of these high-leverage pleiotropic routes of adaptation
795 must be incorporated into our thinking of the evolution of complex systems. Indeed, we
796 commonly think of pleiotropy as purely random, with mutations shifting multiple traits at once in
797 a random and thus largely incoherent way. This generates expectations that pleiotropy should
798 be costly, as such incoherent shifts lead to a generically disorganized state. Given that actual
799 organisms have low-dimensional but pleiotropic signaling and regulatory systems, pleiotropy
800 can often be coherent and thus might often enhance adaptive potential and allow for surprisingly
801 large-effect adaptive mutations. It is therefore important to think of regulation and adaptation as
802 two sides of the same problem of how to change complex and tightly integrated systems in an
803 adaptive manner.

804 REFERENCES

- 805 Aggeli, Dimitra, Yuping Li, and Gavin Sherlock. 2021. "Changes in the Distribution of Fitness Effects and
806 Adaptive Mutational Spectra Following a Single First Step towards Adaptation." *Nature
807 Communications* 12 (1): 5193. <https://doi.org/10.1038/s41467-021-25440-7>.
- 808 Ait-EI-Mkadem, Samira, Manal Dayem-Quere, Mirjana Gusic, Annabelle Chaussenot, Sylvie Bannwarth,
809 Bérengère François, Emmanuelle C. Genin, et al. 2017. "Mutations in MDH2, Encoding a Krebs
810 Cycle Enzyme, Cause Early-Onset Severe Encephalopathy." *American Journal of Human Genetics*
811 100 (1): 151–59. <https://doi.org/10.1016/j.ajhg.2016.11.014>.
- 812 Altschul, S. F., W. Gish, W. Miller, E. W. Myers, and D. J. Lipman. 1990. "Basic Local Alignment Search
813 Tool." *Journal of Molecular Biology* 215 (3): 403–10. [https://doi.org/10.1016/S0022-2836\(05\)80360-2](https://doi.org/10.1016/S0022-2836(05)80360-2).
- 814 Bailey, Matthew H., Collin Tokheim, Eduard Porta-Pardo, Sohini Sengupta, Denis Bertrand, Amila
815 Weerasinghe, Antonio Colaprico, et al. 2018. "Comprehensive Characterization of Cancer Driver
816 Genes and Mutations." *Cell* 173 (2): 371–85.e18. <https://doi.org/10.1016/j.cell.2018.02.060>.
- 817 Bakerlee, Christopher W., Angela M. Phillips, Alex N. Nguyen Ba, and Michael M. Desai. 2021.
818 "Dynamics and Variability in the Pleiotropic Effects of Adaptation in Laboratory Budding Yeast
819 Populations." *eLife* 10 (October). <https://doi.org/10.7554/eLife.70918>.
- 820 *BarcodeCounter2: Count DNA Barcodes Version 2.* n.d. Github. Accessed April 10, 2024.
821 <https://github.com/sandeepvenkataram/BarcodeCounter2>.
- 822 Blount, Zachary D., Christina Z. Borland, and Richard E. Lenski. 2008. "Historical Contingency and the
823 Evolution of a Key Innovation in an Experimental Population of *Escherichia Coli*." *Proceedings of the
824 National Academy of Sciences of the United States of America* 105 (23): 7899–7906.
825 <https://doi.org/10.1073/pnas.0803151105>.
- 826 Boles Eckhard, de Jong-Gubbels Patricia, and Pronk Jack T. 1998. "Identification and Characterization
827 of MAE1, the *Saccharomyces Cerevisiae* Structural Gene Encoding Mitochondrial Malic Enzyme."
828 *Journal of Bacteriology* 180 (11): 2875–82. <https://doi.org/10.1128/jb.180.11.2875-2882.1998>.
- 829 Bono, Lisa M., Leno B. Smith Jr, David W. Pfennig, and Christina L. Burch. 2017. "The Emergence of
830 Performance Trade-Offs during Local Adaptation: Insights from Experimental Evolution." *Molecular
831 Ecology* 26 (7): 1720–33. <https://doi.org/10.1111/mec.13979>.
- 832 Brown, James A., Gavin Sherlock, Chad L. Myers, Nicola M. Burrows, Changchun Deng, H. Irene Wu,
833 Kelly E. McCann, Olga G. Troyanskaya, and J. Martin Brown. 2006. "Global Analysis of Gene
834 Function in Yeast by Quantitative Phenotypic Profiling." *Molecular Systems Biology* 2 (January):
835 2006.0001. <https://doi.org/10.1038/msb4100043>.
- 836 Chaithanya, Koppisetty Viswa, and Himanshu Sinha. 2023. "MKT1 Alleles Regulate Stress Responses
837 through Posttranscriptional Modulation of Puf3 Targets in Budding Yeast." *Yeast* 40 (12): 616–27.
838 <https://doi.org/10.1002/yea.3908>.
- 839 Chang, Yeonji, and Won-Ki Huh. 2018. "Ksp1-Dependent Phosphorylation of eIF4G Modulates Post-
840 Transcriptional Regulation of Specific mRNAs under Glucose Deprivation Conditions." *Nucleic Acids
841 Research* 46 (6): 3047–60. <https://doi.org/10.1093/nar/gky097>.
- 842 Chou, Hsin-Hung, Hsuan-Chao Chiu, Nigel F. Delaney, Daniel Segrè, and Christopher J. Marx. 2011.
843 "Diminishing Returns Epistasis among Beneficial Mutations Decelerates Adaptation." *Science* 332
844 (6034): 1190–92. <https://doi.org/10.1126/science.1203799>.
- 845 Cingolani, Pablo, Adrian Platts, Le Lily Wang, Melissa Coon, Tung Nguyen, Luan Wang, Susan J. Land,
846 Xiangyi Lu, and Douglas M. Ruden. 2012. "A Program for Annotating and Predicting the Effects of
847 Single Nucleotide Polymorphisms, SnpEff: SNPs in the Genome of *Drosophila Melanogaster* Strain
848 w1118; Iso-2; Iso-3." *Fly* 6 (2): 80–92. <https://doi.org/10.4161/fly.19695>.
- 849 DeRisi, J. L., V. R. Iyer, and P. O. Brown. 1997. "Exploring the Metabolic and Genetic Control of Gene
850 Expression on a Genomic Scale." *Science* 278 (5338): 680–86.
851 <https://doi.org/10.1126/science.278.5338.680>.
- 852 Fisher, Kaitlin J., Sean W. Buskirk, Ryan C. Vignogna, Daniel A. Marad, and Gregory I. Lang. 2018.
853 "Adaptive Genome Duplication Affects Patterns of Molecular Evolution in *Saccharomyces
854 Cerevisiae*." *PLoS Genetics* 14 (5): e1007396. <https://doi.org/10.1371/journal.pgen.1007396>.
- 855 Good, Benjamin H., and Michael M. Desai. 2015. "The Impact of Macroscopic Epistasis on Long-Term

- 856 Evolutionary Dynamics." *Genetics* 199 (1): 177–90. <https://doi.org/10.1534/genetics.114.172460>.
- 857 Gupta, Saumya, Aparna Radhakrishnan, Pandu Raharja-Liu, Gen Lin, Lars M. Steinmetz, Julien
858 Gagneur, and Himanshu Sinha. 2015. "Temporal Expression Profiling Identifies Pathways Mediating
859 Effect of Causal Variant on Phenotype." *PLoS Genetics* 11 (6): e1005195.
860 <https://doi.org/10.1371/journal.pgen.1005195>.
- 861 Hanahan, Douglas. 2022. "Hallmarks of Cancer: New Dimensions." *Cancer Discovery* 12 (1): 31–46.
862 <https://doi.org/10.1158/2159-8290.CD-21-1059>.
- 863 Hanahan, Douglas, and Robert A. Weinberg. 2011. "Hallmarks of Cancer: The next Generation." *Cell* 144
864 (5): 646–74. <https://doi.org/10.1016/j.cell.2011.02.013>.
- 865 Harms, Michael J., and Joseph W. Thornton. 2014. "Historical Contingency and Its Biophysical Basis in
866 Glucocorticoid Receptor Evolution." *Nature* 512 (7513): 203–7. <https://doi.org/10.1038/nature13410>.
- 867 Hartwell, L. H., J. J. Hopfield, S. Leibler, and A. W. Murray. 1999. "From Molecular to Modular Cell
868 Biology." *Nature* 402 (6761 Suppl): C47–52. <https://doi.org/10.1038/35011540>.
- 869 Hong, Jungeui, and David Gresham. 2014. "Molecular Specificity, Convergence and Constraint Shape
870 Adaptive Evolution in Nutrient-Poor Environments." *PLoS Genetics* 10 (1): e1004041.
871 <https://doi.org/10.1371/journal.pgen.1004041>.
- 872 Iraqui, I., S. Vissers, B. André, and A. Urrestarazu. 1999. "Transcriptional Induction by Aromatic Amino
873 Acids in *Saccharomyces Cerevisiae*." *Molecular and Cellular Biology* 19 (5): 3360–71.
874 <https://doi.org/10.1128/MCB.19.5.3360>.
- 875 Jasmin, Jean-Nicolas, and Rees Kassen. 2007. "On the Experimental Evolution of Specialization and
876 Diversity in Heterogeneous Environments." *Ecology Letters* 10 (4): 272–81.
877 <https://doi.org/10.1111/j.1461-0248.2007.01021.x>.
- 878 Johnson, Milo S., Shreyas Gopalakrishnan, Juhee Goyal, Megan E. Dillingham, Christopher W. Bakerlee,
879 Parris T. Humphrey, Tanush Jagdish, et al. 2021. "Phenotypic and Molecular Evolution across
880 10,000 Generations in Laboratory Budding Yeast Populations." *eLife* 10 (January).
881 <https://doi.org/10.7554/eLife.63910>.
- 882 Kinsler, Grant, Kerry Geiler-Samerotte, and Dmitri A. Petrov. 2020. "Fitness Variation across Subtle
883 Environmental Perturbations Reveals Local Modularity and Global Pleiotropy of Adaptation." *eLife* 9
884 (December). <https://doi.org/10.7554/eLife.61271>.
- 885 Kinsler, Grant, Kara Schmidlin, Daphne Newell, Rachel Eder, Sam Apodaca, Grace Lam, Dmitri Petrov,
886 and Kerry Geiler-Samerotte. 2023. "Extreme Sensitivity of Fitness to Environmental Conditions:
887 Lessons from #1BigBatch." *Journal of Molecular Evolution* 91 (3): 293–310.
888 <https://doi.org/10.1007/s00239-023-10114-3>.
- 889 Kistler, M., K. Maier, and F. Eckardt-Schupp. 1990. "Genetic and Biochemical Analysis of Glutathione-
890 Deficient Mutants of *Saccharomyces Cerevisiae*." *Mutagenesis* 5 (1): 39–44.
891 <https://doi.org/10.1093/mutage/5.1.39>.
- 892 Komeili, A., K. P. Wedaman, E. K. O'Shea, and T. Powers. 2000. "Mechanism of Metabolic Control.
893 Target of Rapamycin Signaling Links Nitrogen Quality to the Activity of the Rtg1 and Rtg3
894 Transcription Factors." *The Journal of Cell Biology* 151 (4): 863–78.
895 <https://doi.org/10.1083/jcb.151.4.863>.
- 896 Kryazhimskiy, Sergey, Daniel P. Rice, Elizabeth R. Jerison, and Michael M. Desai. 2014. "Microbial
897 Evolution. Global Epistasis Makes Adaptation Predictable despite Sequence-Level Stochasticity." *Science*
898 344 (6191): 1519–22. <https://doi.org/10.1126/science.1250939>.
- 899 Kurita, O., and Y. Nishida. 1999. "Involvement of Mitochondrial Aldehyde Dehydrogenase ALD5 in
900 Maintenance of the Mitochondrial Electron Transport Chain in *Saccharomyces Cerevisiae*." *FEMS
901 Microbiology Letters* 181 (2): 281–87. <https://doi.org/10.1111/j.1574-6968.1999.tb08856.x>.
- 902 Langmead, Ben, and Steven L. Salzberg. 2012. "Fast Gapped-Read Alignment with Bowtie 2." *Nature
903 Methods* 9 (4): 357–59. <https://doi.org/10.1038/nmeth.1923>.
- 904 Lapointe, Christopher P., Jonathan A. Stefely, Adam Jochem, Paul D. Hutchins, Gary M. Wilson, Nicholas
905 W. Kwiecien, Joshua J. Coon, Marvin Wickens, and David J. Pagliarini. 2018. "Multi-Omics Reveal
906 Specific Targets of the RNA-Binding Protein Puf3p and Its Orchestration of Mitochondrial
907 Biogenesis." *Cell Systems* 6 (1): 125–35.e6. <https://doi.org/10.1016/j.cels.2017.11.012>.
- 908 Lee, Chien-Der, and Benjamin P. Tu. 2015. "Glucose-Regulated Phosphorylation of the PUF Protein Puf3

- Regulates the Translational Fate of Its Bound mRNAs and Association with RNA Granules." *Cell Reports* 11 (10): 1638–50. <https://doi.org/10.1016/j.celrep.2015.05.014>.
- Lee, Kyusung, and Ji-Sook Hahn. 2013. "Interplay of Aro80 and GATA Activators in Regulation of Genes for Catabolism of Aromatic Amino Acids in *Saccharomyces Cerevisiae*." *Molecular Microbiology* 88 (6): 1120–34. <https://doi.org/10.1111/mmi.12246>.
- Levy, Sasha F., Jamie R. Blundell, Sandeep Venkataram, Dmitri A. Petrov, Daniel S. Fisher, and Gavin Sherlock. 2015. "Quantitative Evolutionary Dynamics Using High-Resolution Lineage Tracking." *Nature* 519 (7542): 181–86. <https://doi.org/10.1038/nature14279>.
- Liao, X., and R. A. Butow. 1993. "RTG1 and RTG2: Two Yeast Genes Required for a Novel Path of Communication from Mitochondria to the Nucleus." *Cell* 72 (1): 61–71. [https://doi.org/10.1016/0092-8674\(93\)90050-z](https://doi.org/10.1016/0092-8674(93)90050-z).
- Li, Fangfei, Aditya Mahadevan, and Gavin Sherlock. 2023. "An Improved Algorithm for Inferring Mutational Parameters from Bar-Seq Evolution Experiments." *BMC Genomics* 24 (1): 246. <https://doi.org/10.1186/s12864-023-09345-x>.
- Li, Fangfei, Jason Tarkington, and Gavin Sherlock. 2023. "Fit-Seq2.0: An Improved Software for High-Throughput Fitness Measurements Using Pooled Competition Assays." *Journal of Molecular Evolution* 91 (3): 334–44. <https://doi.org/10.1007/s00239-023-10098-0>.
- Li, Heng. 2011. "A Statistical Framework for SNP Calling, Mutation Discovery, Association Mapping and Population Genetical Parameter Estimation from Sequencing Data." *Bioinformatics* 27 (21): 2987–93. <https://doi.org/10.1093/bioinformatics/btr509>.
- Li, Heng, and Richard Durbin. 2009. "Fast and Accurate Short Read Alignment with Burrows–Wheeler Transform." *Bioinformatics* 25 (14): 1754–60. <https://doi.org/10.1093/bioinformatics/btp324>.
- Liu, Zhengchang, Takayuki Sekito, Mário Spírek, Janet Thornton, and Ronald A. Butow. 2003. "Retrograde Signaling Is Regulated by the Dynamic Interaction between Rtg2p and Mks1p." *Molecular Cell* 12 (2): 401–11. [https://doi.org/10.1016/s1097-2765\(03\)00285-5](https://doi.org/10.1016/s1097-2765(03)00285-5).
- Li, Yuping, Dmitri A. Petrov, and Gavin Sherlock. 2019. "Single Nucleotide Mapping of Trait Space Reveals Pareto Fronts That Constrain Adaptation." *Nature Ecology & Evolution* 3 (11): 1539–51. <https://doi.org/10.1038/s41559-019-0993-0>.
- Li, Yuping, Sandeep Venkataram, Atish Agarwala, Barbara Dunn, Dmitri A. Petrov, Gavin Sherlock, and Daniel S. Fisher. 2018. "Hidden Complexity of Yeast Adaptation under Simple Evolutionary Conditions." *Current Biology: CB* 28 (4): 515–25.e6. <https://doi.org/10.1016/j.cub.2018.01.009>.
- McAlister-Henn, L., and L. M. Thompson. 1987. "Isolation and Expression of the Gene Encoding Yeast Mitochondrial Malate Dehydrogenase." *Journal of Bacteriology* 169 (11): 5157–66. <https://doi.org/10.1128/jb.169.11.5157-5166.1987>.
- Melo, Diogo, Arthur Porto, James M. Cheverud, and Gabriel Marroig. 2016. "Modularity: Genes, Development and Evolution." *Annual Review of Ecology, Evolution, and Systematics* 47 (September): 463–86. <https://doi.org/10.1146/annurev-ecolsys-121415-032409>.
- Murphy, J. Patrick, Ekaterina Stepanova, Robert A. Everley, Joao A. Paulo, and Steven P. Gygi. 2015. "Comprehensive Temporal Protein Dynamics during the Diauxic Shift in *Saccharomyces Cerevisiae*." *Molecular & Cellular Proteomics: MCP* 14 (9): 2454–65. <https://doi.org/10.1074/mcp.M114.045849>.
- Navarro-Aviño, J. P., R. Prasad, V. J. Miralles, R. M. Benito, and R. Serrano. 1999. "A Proposal for Nomenclature of Aldehyde Dehydrogenases in *Saccharomyces Cerevisiae* and Characterization of the Stress-Inducible ALD2 and ALD3 Genes." *Yeast* 15 (10A): 829–42. [https://doi.org/10.1002/\(SICI\)1097-0061\(199907\)15:10A<829::AID-YEA423>3.0.CO;2-9](https://doi.org/10.1002/(SICI)1097-0061(199907)15:10A<829::AID-YEA423>3.0.CO;2-9).
- Orr, H. A. 2000. "Adaptation and the Cost of Complexity." *Evolution; International Journal of Organic Evolution* 54 (1): 13–20. <https://doi.org/10.1111/j.0014-3820.2000.tb00002.x>.
- Park, Yeonwoo, Brian P. H. Metzger, and Joseph W. Thornton. 2022. "Epistatic Drift Causes Gradual Decay of Predictability in Protein Evolution." *Science* 376 (6595): 823–30. <https://doi.org/10.1126/science.abn6895>.
- Lawson, T., and N. Warner. 2007. "Oncogenic Re-Wiring of Cellular Signaling Pathways." *Oncogene* 26 (9): 1268–75. <https://doi.org/10.1038/sj.onc.1210255>.
- Reinders, Jörg, Karina Wagner, Rene P. Zahedi, Diana Stojanovski, Beate Eyrich, Martin van der Laan, Peter Rehling, Albert Sickmann, Nikolaus Pfanner, and Chris Meisinger. 2007. "Profiling

- 962 Phosphoproteins of Yeast Mitochondria Reveals a Role of Phosphorylation in Assembly of the ATP
963 Synthase*." *Molecular & Cellular Proteomics: MCP* 6 (11): 1896–1906.
964 <https://doi.org/10.1074/mcp.M700098-MCP200>.
- 965 Repetto, B., and A. Tzagoloff. 1989. "Structure and Regulation of KGD1, the Structural Gene for Yeast
966 Alpha-Ketoglutarate Dehydrogenase." *Molecular and Cellular Biology* 9 (6): 2695–2705.
967 <https://doi.org/10.1128/mcb.9.6.2695-2705.1989>.
- 968 Sanchez-Vega, Francisco, Marco Mina, Joshua Armenia, Walid K. Chatila, Augustin Luna, Konnor C. La,
969 Sofia Dimitriadou, et al. 2018. "Oncogenic Signaling Pathways in The Cancer Genome Atlas." *Cell*
970 173 (2): 321–37.e10. <https://doi.org/10.1016/j.cell.2018.03.035>.
- 971 Schlossarek, Dennis, Marcin Luzarowski, Ewelina M. Sokołowska, Venkatesh P. Thirumalaikumar, Lisa
972 Dengler, Lothar Willmitzer, Jennifer C. Ewald, and Aleksandra Skirycz. 2022. "Rewiring of the
973 Protein-Protein-Metabolite Interactome during the Diauxic Shift in Yeast." *Cellular and Molecular Life*
974 *Sciences: CMLS* 79 (11): 550. <https://doi.org/10.1007/s00018-022-04569-8>.
- 975 Sekito, Takayuki, Zhengchang Liu, Janet Thornton, and Ronald A. Butow. 2002. "RTG-Dependent
976 Mitochondria-to-Nucleus Signaling Is Regulated by MKS1 and Is Linked to Formation of Yeast Prion
977 [URE3]." *Molecular Biology of the Cell* 13 (3): 795–804. <https://doi.org/10.1091/mbc.01-09-0473>.
- 978 Sekito, T., J. Thornton, and R. A. Butow. 2000. "Mitochondria-to-Nuclear Signaling Is Regulated by the
979 Subcellular Localization of the Transcription Factors Rtg1p and Rtg3p." *Molecular Biology of the Cell*
980 11 (6): 2103–15. <https://doi.org/10.1091/mbc.11.6.2103>.
- 981 Sondka, Zbyslaw, Sally Bamford, Charlotte G. Cole, Sari A. Ward, Ian Dunham, and Simon A. Forbes.
982 2018. "The COSMIC Cancer Gene Census: Describing Genetic Dysfunction across All Human
983 Cancers." *Nature Reviews. Cancer* 18 (11): 696–705. <https://doi.org/10.1038/s41568-018-0060-1>.
- 984 Suissa, M., K. Suda, and G. Schatz. 1984. "Isolation of the Nuclear Yeast Genes for Citrate Synthase and
985 Fifteen Other Mitochondrial Proteins by a New Screening Method." *The EMBO Journal* 3 (8): 1773–
986 81. <https://doi.org/10.1002/j.1460-2075.1984.tb02045.x>.
- 987 Tung, Sudipta, Christopher W. Bakerlee, Angela M. Phillips, Alex N. Nguyen Ba, and Michael M. Desai.
988 2021. "The Genetic Basis of Differential Autodiploidization in Evolving Yeast Populations." *G3* 11 (8).
989 <https://doi.org/10.1093/g3journal/jkab192>.
- 990 Umekawa, Midori, and Daniel J. Klionsky. 2012. "Ksp1 Kinase Regulates Autophagy via the Target of
991 Rapamycin Complex 1 (TORC1) Pathway." *The Journal of Biological Chemistry* 287 (20): 16300–
992 310. <https://doi.org/10.1074/jbc.M112.344952>.
- 993 Van der Auwera, Geraldine A., and Brian D. O'Connor. 2020. *Genomics in the Cloud: Using Docker,*
994 *GATK, and WDL in Terra.* "O'Reilly Media, Inc."
995 <https://play.google.com/store/books/details?id=vsXaDwAAQBAJ>.
- 996 Venkataram, Sandeep, Barbara Dunn, Yuping Li, Atish Agarwala, Jessica Chang, Emily R. Ebel, Kerry
997 Geiler-Samerotte, et al. 2016. "Development of a Comprehensive Genotype-to-Fitness Map of
998 Adaptation-Driving Mutations in Yeast." *Cell* 166 (6): 1585–96.e22.
999 <https://doi.org/10.1016/j.cell.2016.08.002>.
- 1000 Wagner, Günter P., and Lee Altenberg. 1996. "PERSPECTIVE: COMPLEX ADAPTATIONS AND THE
1001 EVOLUTION OF EVOLVABILITY." *Evolution; International Journal of Organic Evolution* 50 (3): 967–
1002 76. <https://doi.org/10.1111/j.1558-5646.1996.tb02339.x>.
- 1003 Wagner, Günter P., Mihaela Pavlicev, and James M. Cheverud. 2007. "The Road to Modularity." *Nature*
1004 *Reviews. Genetics* 8 (12): 921–31. <https://doi.org/10.1038/nrg2267>.
- 1005 Wagner, Günter P., and Jianzhi Zhang. 2011. "The Pleiotropic Structure of the Genotype-Phenotype Map:
1006 The Evolvability of Complex Organisms." *Nature Reviews. Genetics* 12 (3): 204–13.
1007 <https://doi.org/10.1038/nrg2949>.
- 1008 Welch, John J., and David Waxman. 2003. "Modularity and the Cost of Complexity." *Evolution;*
1009 *International Journal of Organic Evolution* 57 (8): 1723–34. [3820.2003.tb00581.x](https://doi.org/10.1111/j.0014-
1010 3820.2003.tb00581.x).
- 1011 Wilson, Wayne A., and Peter J. Roach. 2002. "Nutrient-Regulated Protein Kinases in Budding Yeast." *Cell*
1012 111 (2): 155–58. [https://doi.org/10.1016/s0092-8674\(02\)01043-7](https://doi.org/10.1016/s0092-8674(02)01043-7).
- 1013 Wiser, Michael J., Noah Ribeck, and Richard E. Lenski. 2013. "Long-Term Dynamics of Adaptation in
1014 Asexual Populations." *Science* 342 (6164): 1364–67. <https://doi.org/10.1126/science.1243357>.

- 1015 Wünsche, Andrea, Duy M. Dinh, Rebecca S. Satterwhite, Carolina Diaz Arenas, Daniel M. Stoebel, and
1016 Tim F. Cooper. 2017. "Diminishing-Returns Epistasis Decreases Adaptability along an Evolutionary
1017 Trajectory." *Nature Ecology & Evolution* 1 (4): 61. <https://doi.org/10.1038/s41559-016-0061>.
- 1018 Zampar, Guillermo G., Anne Kümmel, Jennifer Ewald, Stefan Jol, Bastian Niebel, Paola Picotti, Ruedi
1019 Aebersold, Uwe Sauer, Nicola Zamboni, and Matthias Heinemann. 2013. "Temporal System-Level
1020 Organization of the Switch from Glycolytic to Gluconeogenic Operation in Yeast." *Molecular Systems
1021 Biology* 9: 651. <https://doi.org/10.1038/msb.2013.11>.

1022 **METHODS**

1023

1024 **Constructing barcoded populations from first-step mutants**

1025 To conduct second-step evolution experiments, we constructed barcoded populations for each
1026 of five mutations (see table 1) that arose in the original 2-Day evolution experiment (Levy et al.
1027 2015). Construction of the barcoded populations of *CYR1*, *GPB2*, and *TOR1* mutations was
1028 previously described (Aggeli, Li, and Sherlock 2021). To barcode *IRA1-nonsense* and *IRA1-*
1029 *missense* mutants, we followed a similar procedure. Specifically, we backcrossed the *IRA1*
1030 mutants (*MAT α*) to GSY5375, a *MAT α* ancestral S288C strain that harbors the pre-landing pad
1031 locus (Aggeli, Li, and Sherlock 2021). After sporulation and tetrad dissection, we performed
1032 Sanger sequencing to identify segregants that were *MAT α* , carried the *IRA1* variant of interest,
1033 and the pre-landing pad allele at the barcode locus, ensuring the removal of the barcode initially
1034 labeling this strain. These segregants were used for downstream transformation of barcodes.

1035

1036 We then barcoded these strains with a low and high complexity barcode as described in Aggeli
1037 et al. We first transformed in the low-complexity barcode by PCR-amplifying a region from the
1038 L001 library, which harbors a NatMX selectable marker, half of *URA3*, an artificial intron, a low-
1039 complexity barcode sequence, and a lox66 site. We then selected for successful transformants
1040 using YPD + Nat plates and isolated 4 and 8 colonies for *IRA1-missense* and *IRA1-nonsense*
1041 strains, respectively, each with a unique low-complexity barcode. For each of these strains, we
1042 then transformed a library of high-complexity barcodes (pBAR3). After transformation, cells
1043 were grown in YP + 2% galactose for 16hrs to induce Cre recombinase expression prior to
1044 selection on SC-ura plates with 2% glucose. We then estimated the number of unique
1045 transformants by counting the number of colonies grown from plating a dilution. We additionally
1046 estimated the relative number of unique transformants by amplicon Illumina sequencing using
1047 the sequencing primers described below.

1048

1049 To construct populations for evolution experiments, we pooled together transformants from
1050 multiple high-complexity transformations, such that each barcode was equally represented in
1051 each pool. This resulted in pools of ~100,000 high-complexity barcodes for each evolution
1052 experiment with the exception of Evo2D *IRA1-missense* evolution pool which contained ~40,000
1053 high-complexity barcodes. Transformants were pooled such that each low-complexity barcode
1054 was only present in one evolution pool, allowing us later to identify evolution conditions based
1055 on the identity of the low-complexity barcode. For Evo1D experiments, a pool of *IRA1-missense*
1056 and *IRA1-nonsense* transformants was used, containing equal numbers in abundance, albeit
1057 with ~32,000 unique *IRA1-missense* barcodes and ~60,000 *IRA1-nonsense* barcodes. A single
1058 pool that contained barcoded populations of *CYR1*, *GPB2*, and *TOR1* mutants was used for the
1059 second-step Evo1D and Evo3D experiments for these genotypes.

1060

1061 **Conducting evolution experiments.**

1062 We conducted evolution experiments with barcoded populations under identical conditions to
1063 the original evolution experiment. Briefly, ~10⁸ cells of each evolution population pool was

1064 inoculated in 50 mL of SC-ura + 2% dextrose + hygromycin in 500 mL Delong flasks and grown
1065 overnight at 30°C with shaking at 223 rpm. 500 µL of saturated overnight culture was then
1066 transferred to 100 mL of glucose-limited M3 medium (5x delft medium with 4% ammonium
1067 sulfate and 1.5% dextrose) in 500 mL Delong flasks for the evolution experiment. For most of
1068 the evolution experiments, the culture was split into 2 replicate flasks at this point. Second-step
1069 Evo3D experiments from *IRA1-missense* or *IRA1-nonsense* mutants used 3 replicates each.
1070 Cultures then propagated every 24, 48, or 72 hours for Evo1D, Evo2D, and Evo3D conditions,
1071 respectively. At the time of transfer, a set volume was transferred into 100 mL of fresh medium.
1072 In order to keep the bottleneck size consistent at ~5x10⁷ viable cells, the volume varied by
1073 condition. Evo2D conditions used 400 µl of transfer volume. Evo1D and Evo3D conditions used
1074 500 µL of transfer volume, which accounted for decreased cell density and decreased cell
1075 viability in these conditions, respectively. Two 1 mL volumes of saturated culture were frozen as
1076 glycerol stocks. The remaining culture was spun down, resuspended in 5 mL of sorbitol freezing
1077 solution (0.9M sorbitol, 100mM Tris pH 7.5, 100mM EDTA) and frozen at -20°C for subsequent
1078 genomic DNA extraction and barcode library sequencing preparation.

1079

1080 **Isolation of clones from evolution experiments.**

1081

1082 To isolate clones for fitness measurement experiments, quantification of growth phase
1083 performances, and whole genome sequencing, we sorted individual cells as previously
1084 described (Y. Li, Petrov, and Sherlock 2019) . Specifically, we sorted 480 individual cells (five
1085 96-well plates) from each replicate evolution experiment into single wells of a 96-well plate with
1086 100 µL of YPD medium. This resulted in a total of 80 plates (~7,680 sorted cells) across the 16
1087 evolution experiments. Sorted cells were then grown at 30°C for 3 days without shaking until the
1088 cells reached saturation. Saturated cultures (5µl) were then transferred to deep-well 96-well
1089 plates with 300 µL of YPD. After 2 days of growth at 30°C without shaking, 100 µL of culture
1090 were mixed with glycerol and frozen at -80°C. 20 µL of saturated culture were transferred to 96-
1091 well PCR plates and frozen at -20°C. for barcode identification. Saturated culture was also
1092 plated onto Benomyl plates to assay ploidy (Venkataram et al. 2016).

1093

1094 *Barcode identification by Metagrid.*
1095 To identify the barcode associated with each well and ensure that multiple clones with the same
1096 barcode were not kept for downstream fitness measurement experiments, we performed
1097 sequencing on the barcodes of the clones in each well. Saturated culture (20µl) was transferred
1098 to 96-well plates and frozen at -20°C. Cells were then lysed by incubation at 95°C for 15 min. 5
1099 µL of lysed culture were used as the template for PCR amplification of the barcode region. We
1100 performed two steps of PCR. In the first-step of PCR, we used a set of 72 forward and 64
1101 reverse first-step primers, each with a unique 8-bp multiplexing tag, to combinatorially label
1102 each well. After the first-step of PCR, 5 µL of each well's PCR product from 5 plates was pooled
1103 together and the appropriate 250bp band was isolated using gel purification. A second-step of
1104 PCR was then performed with standard Nextera primers. Amplicon libraries were then
1105 sequenced on Illumina MiSeq or HiSeq machines.

1106
1107 To computationally identify the barcodes associated with each well, we used BarcodeCounter2
1108 to extract the multiplexing indexes and barcode regions from each read. We then associated
1109 barcodes with each well by taking the barcode with the most reads per well, provided the well
1110 had at least 200 reads, the barcode was at least 60% of the well's reads, and it received more
1111 than 1.5x the second-highest barcode in the well. This resulted in identifying the locations of
1112 1785 unique barcoded clones. This is lower than the highest possible number of 7,680 clones
1113 due to a combination of some wells receiving multiple clones, multiple wells receiving cells of
1114 the same barcode, and drop out due to sequencing depth. To further validate our approach, we
1115 randomly selected 3 wells per plate and performed Sanger sequencing of their barcodes. Of the
1116 wells where both barcodes were identified using the metagrid approach and Sanger reads were
1117 of sufficiently high quality, over 85% of the barcodes matched. We subsequently pooled each
1118 uniquely barcoded clone by evolution condition and parental strain, resulting in 4 pools of
1119 barcoded lineages to be used for fitness measurement experiments.
1120

1121 *Benomyl ploidy test.*

1122 To characterize the ploidy of each sorted clone, we performed a high-throughput ploidy test that
1123 was previously developed (Venkataram et al. 2016). Saturated culture from cell sorting was
1124 pinned onto YPD agar plates containing 20 mg/mL benomyl. Plates were then grown at 25°C for
1125 2 days and then imaged. Clones with inhibited growth on the benomyl medium were identified
1126 as diploids. Clones with normal growth on the benomyl medium were identified as haploids. See
1127 "Mutation and ploidy classification" section below.
1128

1129 **Constructing barcoded pools**

1130 To construct a pool of lineages for fitness measurement experiments, we generated one large
1131 pool of barcoded lineages isolated from previous evolution experiments and the evolution
1132 experiments described in this study. Briefly, one tube of each barcode pool was thawed and
1133 grown in YPD at 30°C overnight. After the overnight growth, we pooled all barcode-sub pools
1134 together, adjusting for the number of barcodes in each pool and the OD600 of the culture, such
1135 that each barcode was equally represented in this big pool. This big pool was then split into 1
1136 mL glycerol stock aliquots and frozen at -80°C.
1137

1138 To precisely measure the mean fitness of the population, we constructed two pools of 60 neutral
1139 lineages from Venkataram 2016 and Li 2019. Briefly, we identified barcodes that exhibited
1140 neutral fitness estimates across all previous experiments done with these pools of barcoded
1141 lineages (Venkataram et al. 2016; Y. Li et al. 2018; Y. Li, Petrov, and Sherlock 2019; Kinsler,
1142 Geiler-Samerotte, and Petrov 2020). We then streaked out from glycerol stocks onto YPD
1143 plates. A single colony was picked from each barcoded lineage and grown in 96-well deep-well
1144 plates for 2 days. Wells for each collection of 60 neutrals were then pooled equally by volume.
1145 Then, glycerol stocks were created with 1 mL of pooled culture and frozen at -80°C.

1146
1147 **Fitness measurement experiments**
1148 To quantify fitness effects, we performed fitness measurement experiments. We streaked out
1149 DPY256 (an ancestor strain which harbors an ApaLI restriction site in the barcode region) onto
1150 a YPD plate. After two days of growth, a colony was picked and grown up in 50 mL of YPD
1151 overnight. Additionally, one tube each of the 60-neutral pool from Venkataram 2016 and one
1152 tube of the 60-neutral pool from the Li 2019 pool was thawed and grown separately in 50 mL of
1153 YPD overnight.
1154
1155 5x10⁷ cells from DPY256 ancestor, each of the two neutral pools, and the big pool (see
1156 Constructing barcoded pools) were then separately inoculated into four 500 mL Delong flasks
1157 containing 100 mL of M3 medium for one cycle of pre-culture in the selective condition. This
1158 resulted in a total of 16 flasks of culture, corresponding to each set of barcoded cells and the
1159 four conditions.
1160
1161 After one cycle of growth (which corresponded to 24h for the 1-Day transfer condition, 48h for 2-
1162 Day, 72h for 3-Day, and 120h for 5-Day), the cultures were pooled by volume such that the big
1163 pool of barcoded lineages represented 2% or 5% of the population. In the 2% flasks, 2% of the
1164 population was the big pool of evolved lineages, 2% were Venkataram 2016 neutrals, 2% were
1165 Li 2019 neutrals, and 94% of the population was DPY256 ancestor. In the 5% flasks, 5% of the
1166 population was the big pool of evolved lineages, 2% were Venkataram 2016 neutrals, 2% were
1167 Li 2019 neutrals, and 91% of the population was DPY256 ancestor. These pools of lineages is
1168 considered “Timepoint 0” for each condition and pooling percentage.
1169
1170 We then transferred a set volume of this pool to replicate flasks (2 replicates for 1- and 2-Day
1171 experiments, 3 replicates for 3- and 5-Day experiments) containing 100 mL M3 medium such
1172 that ~5x10⁷ of viable cells were transferred. This volume was 500 µL for 1-, 3-, and 5-Day
1173 experiments and 400 µL for 2-Day experiments. The culture was then grown at 30°C in an
1174 incubator shaking at 223 RPM. After the set amount of time corresponding to each condition, a
1175 fixed volume of culture (500 µL for 1-, 3-, and 5-Day experiments and 400 µL for 2-Day
1176 experiments) to fresh 100 mL of M3 medium in 500 mL DeLong flasks. This serial dilution was
1177 continued for until transfer 6 for 1- and 2-Day experiments and until transfer 2 for 3- and 5-Day
1178 experiments.
1179
1180 After each transfer, the remaining culture was frozen for downstream DNA extraction, barcode
1181 amplification, and sequencing. To freeze the culture, we transferred the culture to 50 mL conical
1182 tubes, spun down at 3000 rpm for 5 min, resuspending in 5 mL sorbitol freezing solution (0.9 M
1183 sorbitol, 0.1 M Tris-HCL pH 7.5, 0.1 M EDTA pH 8.0), aliquoted into three 1.5 mL tubes, and
1184 stored at -80°C.
1185

1186 **Genomic DNA extraction**

1187 Genomic DNA was extracted from frozen cells as described previously (Aggeli, Li, and Sherlock
1188 2021). Briefly, 400 µL of frozen cells in sorbitol solution was spun down at 3500 rpm for 3 min.
1189 After discarding the supernatant, the cell pellet was then washed in 400 µL of sterile water and
1190 spun down at 3500 rpm for 3 min and the supernatant was discarded. The cell pellet was then
1191 re-suspended in 400 µL of extraction buffer (0.9 M sorbitol, 50 mM Na phosphate pH 7.5,
1192 240 µg/mL zymolase, 14 mM β-mercaptoethanol) and incubated at 37°C for 30min. We then
1193 added 40 µL of 0.5 M EDTA, 40 µL of 10% SDS, and 56 µL of proteinase K (Life Technologies
1194 25530-015), vortexing after each addition. The mixture was then incubated at 65°C for 30 min.
1195 After the incubation, tubes were placed on ice for 5 min and then 200 µL of 5 M potassium
1196 acetate were added and tubes were shaken to mix. Following a 30 min incubation on ice, the
1197 samples were spun for 10 min at 17,000 rpm. The supernatant was transferred to a new 1.5 mL
1198 tube containing 750 µL of isopropanol and placed on ice for 5 min. We then spun the samples at
1199 17,000 rpm for 10min and discarded the supernatant. The DNA pellet was then washed twice
1200 with 750 µL 70% ethanol, each time vortexing very briefly, spun at 17,000 rpm for 2 min, and
1201 discarding the supernatant. After allowing the DNA pellet to dry completely, it was resuspended
1202 in 50 µl 10 mM Tris ph 7.5 or 50 µL nuclease free water. We then added 1 µL of 20 mg/mL
1203 RNase A and subsequently incubated at 65°C for 30 min. DNA was then quantified using the
1204 Qubit Range dsDNA assay kit.

1205

1206 **Restriction digest of ancestral strain's barcode**

1207 Because over 90% of the initial population during the fitness measurement experiments consists
1208 of the ancestral strain, we sought to reduce the proportion of reads that represented its barcode
1209 to reduce sequencing costs. We thus performed restriction digestion using the ApaLI restriction
1210 site (GTGCAC) engineered into the barcode region of the DPY256 ancestral strain on DNA for
1211 each sample prior to (and following) PCR amplification. We added 1 µL of ApaLI (NEB
1212 #R0507L) and 5.5 µL of Cutsmart Buffer (NEB #R0507L) to genomic DNA and incubated at
1213 37°C for at least 1hr. Note that no barcode strains besides the ancestral strain contain this
1214 restriction site, due to the design of the barcode region.

1215

1216 **Barcode sequencing library preparation**

1217 To prepare sequencing libraries of the barcodes, we used a two-step PCR amplification
1218 protocol, as previously described (Venkataram et al. 2016; Kinsler, Geiler-Samerotte, and
1219 Petrov 2020; Y. Li et al. 2018). In the first step of PCR, we use HPLC-purified primers that
1220 contain “inline indices” to label samples and 8-bp Unique Molecular Identifiers (UMIs) to identify
1221 barcode reads from the same yeast cell that have been sequenced multiple times due to PCR
1222 amplification.

1223

1224

1225 Step 1 forward primers:

F201	TCGTCGGCAGCGTC AGATGTGTATAAGAGACAG (N1:25252525)(N1)(N1) (N1)(N1) (N1)(N1)CGATGTT TAATATGGACTAAAGGAGGCTTT
F202	TCGTCGGCAGCGTC AGATGTGTATAAGAGACAG (N1:25252525)(N1)(N1) (N1)(N1) (N1)(N1)ACAGTGT TAATATGGACTAAAGGAGGCTTT
F203	TCGTCGGCAGCGTC AGATGTGTATAAGAGACAG (N1:25252525)(N1)(N1) (N1)(N1) (N1)(N1)TGACCAT TAATATGGACTAAAGGAGGCTTT
F204	TCGTCGGCAGCGTC AGATGTGTATAAGAGACAG (N1:25252525)(N1)(N1) (N1)(N1) (N1)(N1)GCCAATT TAATATGGACTAAAGGAGGCTTT
F205	TCGTCGGCAGCGTC AGATGTGTATAAGAGACAG (N1:25252525)(N1)(N1) (N1)(N1) (N1)(N1)ATCACGT TAATATGGACTAAAGGAGGCTTT
F206	TCGTCGGCAGCGTC AGATGTGTATAAGAGACAG (N1:25252525)(N1)(N1) (N1)(N1) (N1)(N1)CAGATCT TAATATGGACTAAAGGAGGCTTT
F207	TCGTCGGCAGCGTC AGATGTGTATAAGAGACAG (N1:25252525)(N1)(N1) (N1)(N1) (N1)(N1)TAGCTTT TAATATGGACTAAAGGAGGCTTT
F208	TCGTCGGCAGCGTC AGATGTGTATAAGAGACAG (N1:25252525)(N1)(N1) (N1)(N1) (N1)(N1)TAGGCT TAATATGGACTAAAGGAGGCTTT
F209	TCGTCGGCAGCGTC AGATGTGTATAAGAGACAG (N1:25252525)(N1)(N1) (N1)(N1) (N1)(N1)TTAGGCT TAATATGGACTAAAGGAGGCTTT
F210	TCGTCGGCAGCGTC AGATGTGTATAAGAGACAG (N1:25252525)(N1)(N1) (N1)(N1) (N1)(N1)ACTTGAT TAATATGGACTAAAGGAGGCTTT
F211	TCGTCGGCAGCGTC AGATGTGTATAAGAGACAG (N1:25252525)(N1)(N1) (N1)(N1) (N1)(N1)GATCACT TAATATGGACTAAAGGAGGCTTT
F212	TCGTCGGCAGCGTC AGATGTGTATAAGAGACAG (N1:25252525)(N1)(N1) (N1)(N1) (N1)(N1)CTTGTAT TAATATGGACTAAAGGAGGCTTT

1226

1227 Step 1 reverse primers:

R301	GTCTCGTGGGCTCGG AGATGTGTATAAGAGACAG (N1:25252525)(N1)(N1) (N1)(N1)(N1)TATATACGC TCGAATTCAAGCTTAGATCTGATA
R302	GTCTCGTGGGCTCGG AGATGTGTATAAGAGACAG (N1:25252525)(N1)(N1) (N1)(N1)(N1)CGCTCTATC TCGAATTCAAGCTTAGATCTGATA
R303	GTCTCGTGGGCTCGG AGATGTGTATAAGAGACAG (N1:25252525)(N1)(N1) (N1)(N1)(N1) (N1)(N1)GAGACGCT TCGAATTCAAGCTTAGATCTGATA
R304	GTCTCGTGGGCTCGG AGATGTGTATAAGAGACAG (N1:25252525)(N1)(N1) (N1)(N1)(N1) (N1)(N1)ATACTGCGT TCGAATTCAAGCTTAGATCTGATA
R305	GTCTCGTGGGCTCGG AGATGTGTATAAGAGACAG (N1:25252525)(N1)(N1) (N1)(N1)(N1) (N1)(N1)ACTAGCAGA TCGAATTCAAGCTTAGATCTGATA
R306	GTCTCGTGGGCTCGG AGATGTGTATAAGAGACAG (N1:25252525)(N1)(N1) (N1)(N1)(N1) (N1)(N1)TGAGCTAGC TCGAATTCAAGCTTAGATCTGATA
R307	GTCTCGTGGGCTCGG AGATGTGTATAAGAGACAG (N1:25252525)(N1)(N1) (N1)(N1)(N1) (N1)(N1)CTGCTACTC TCGAATTCAAGCTTAGATCTGATA
R308	GTCTCGTGGGCTCGG AGATGTGTATAAGAGACAG (N1:25252525)(N1)(N1) (N1)(N1)(N1)CGTAGCGA TCGAATTCAAGCTTAGATCTGATA

1228

1229 For the first step for PCR, we performed 8 or 16 reactions per sample, using ~4.8ug (ranging
 1230 between 3ug and 7.5ug) of DNA per sample across all reactions. Each set of eight 50 μ L
 1231 reactions included 16 μ l of 50mM MgCl₂, 8 μ L of 10 μ M forward primer, 8 μ L of 10 μ M reverse
 1232 primer, template DNA, and 200 μ L of OneTaq HotStart 2X Master mix (NEB #M0484L). Three
 1233 cycles of PCR was then carried out with the following steps:

1. 94°C for 10min
2. 94°C for 3min
3. 55°C for 1min
4. 68°C for 1 min
5. Repeat steps 2-4 twice for a total of 3 cycles
6. 68°C for 1min
7. Hold at 4°C

1241

1242 The first-step PCR product was then column purified using the GeneJET Gel Extraction Kit
 1243 (#K0692). Briefly, 100 μ L of orange binding buffer were added to each 50 μ L reaction. All 8 or
 1244 16 reactions from a given sample were pooled into the same purification column in a vacuum
 1245 manifold. We then washed the column with 750 μ L of wash buffer over vacuum. Then, each
 1246 column was spun for 30s at max speed to remove residual wash buffer. We then eluted into 47
 1247 μ L of nuclease free water by centrifuging and stored the samples at 4°C for the second step of
 1248 PCR.

1249

1250 The second step of PCR further amplifies the barcodes and attaches Illumina indices as well as
 1251 P5, P7 sequences for compatibility with Illumina sequencing, as done previously (Kinsler,
 1252 Geiler-Samerotte, and Petrov 2020; Kinsler et al. 2023). We used Nextera Index Xt v2 primers
 1253 (Illumina #FC-131–2004) with the following sequences:

1254

S513	AATGATAACGGCACCACCGAGATCTACACTCGACTAGTCGTCGGCAGCGTC
S515	AATGATAACGGCACCACCGAGATCTACACTCTAGCTTCGTCCGCAGCGTC
S516	AATGATAACGGCACCACCGAGATCTACACCCTAGAGTTCGTCCGCAGCGTC
S517	AATGATAACGGCACCACCGAGATCTACACCGTAAGATCGTCGGCAGCGTC
S518	AATGATAACGGCACCACCGAGATCTACACCTATTAAAGTCGTCCGCAGCGTC
S520	AATGATAACGGCACCACCGAGATCTACACAGGCTATTCTCGTCCGCAGCGTC
S521	AATGATAACGGCACCACCGAGATCTACACGAGCCTATCGTCGGCAGCGTC
S522	AATGATAACGGCACCACCGAGATCTACACTTATCGATCGTCGGCAGCGTC
N716	CAAGCAGAAGACGGCATACGAGATTAGCGAGTTAGCTCGTGGGCTCGG
N718	CAAGCAGAAGACGGCATACGAGATGAGTGTAGCTCCGTCTCGTGGGCTCGG
N719	CAAGCAGAAGACGGCATACGAGATTACTACGCGTCTCGTGGGCTCGG
N720	CAAGCAGAAGACGGCATACGAGATAGGCTCCGTCTCGTGGGCTCGG
N721	CAAGCAGAAGACGGCATACGAGATGCGTAGTCTCGTGGGCTCGG
N722	CAAGCAGAAGACGGCATACGAGATCTGCGCATGTCGTGGGCTCGG
N723	CAAGCAGAAGACGGCATACGAGATGAGCGCTAGTCTCGTGGGCTCGG
N724	CAAGCAGAAGACGGCATACGAGATCGCAGTGTCTCGTGGGCTCGG
N726	CAAGCAGAAGACGGCATACGAGATGCTTAGGGCTCGTGGGCTCGG
N727	CAAGCAGAAGACGGCATACGAGATACTGATCGGTCTCGTGGGCTCGG
N728	CAAGCAGAAGACGGCATACGAGATTAGCTCGAGTCTCGTGGGCTCGG
N729	CAAGCAGAAGACGGCATACGAGATGACGTCGAGTCTCGTGGGCTCGG

1255

1256 Note that because of increased risk of index swapping associated with sequencing amplicons
 1257 on Illumina machines with ExAmp technology (Kinsler et al. 2023), we labeled each sample with
 1258 a unique combination of inline and Illumina indices. This allows for reads associated with index
 1259 swapping due to mis-incorporation of indices or template swapping on the sequencing machine
 1260 to be identified and removed from downstream analysis.

1261

1262 For the second step of PCR, we performed 3 reactions per sample. For each set of the 50 µL
 1263 reactions, we used 45 µL of column purified Step 1 PCR product, 2.5 µL of the designated
 1264 forward Nextera XT Index V2 primer (e.g., N716), 2.5 µL of the designated reverse Nextera XT
 1265 Index V2 primer (e.g., S513), 3 µL of 10mM dNTP (Fisher Scientific #PR-U1515), 1.5 µL of Q5
 1266 polymerase (NEB #M0491L), 30 µL of Q5 buffer (NEB #M0491L), and 65.5 µL of nuclease free
 1267 water. We then ran the following program on the thermocycler to amplify for 20 cycles:

1268

1. 98°C 30s
2. 98°C 10s
3. 62°C 20s
4. 72°C 30s
5. Repeat steps 2-4 19 times (20 cycles total)
6. 72°C 3min
7. Hold at 4 C

1269

1270 We then performed column purification following a similar procedure to the purification from step
 1271 1, eluting instead into 30 µL of nuclease free water.

1272

1273 Following the second step of PCR, in order to further remove any residual ancestral barcode
 1274 that were not digested before PCR amplification, we performed a second round of ApaLI
 1275 digestion, adding 3.5 µL of Cutsmart buffer and 1 µL of ApaLI restriction enzyme (NEB

1283 #R0507L) to each sample's Step 2 PCR product, digesting for at least 1 hr at 37°C. We then
1284 performed gel extraction using the GeneJet gel purification kit for each sample, keeping the
1285 350bp band representing intact barcode sequences. We then quantified the DNA concentration
1286 for each sample using Qubit HS kit (ThermoFisher #Q32854), pooled such that each sample
1287 was equally represented in the final library, and submitted for sequencing on Illumina
1288 sequencing machines.

1289

1290 **Tracking evolution**

1291 To track the dynamics of the evolution experiment, estimate the fitness of lineages during the
1292 evolution experiment, and infer the distribution of fitness effects, we extracted DNA and used
1293 PCR amplification to generate libraries for sequencing as described above, with the exception of
1294 not performing the ApaLI restriction digestion.

1295

1296 In order to identify barcode counts over time, we followed previously used custom scripts along
1297 with bartender ([https://github.com/Sherlock-
1298 Lab/Barcode_seq/blob/master/bartender_BC1_BC2.py](https://github.com/Sherlock-Lab/Barcode_seq/blob/master/bartender_BC1_BC2.py)) to extract and cluster barcodes from
1299 timepoints along the evolution trajectory.

1300

1301 To infer fitness effects, the mean fitness of the population, and infer the from the evolution
1302 experiments themselves, we used FitMut1 (Levy et al. 2015; F. Li, Mahadevan, and Sherlock
1303 2023). To infer the distribution of fitness effects from this data, we used an approach developed
1304 in Levy et al 2015. The general idea of this approach is to infer the distribution of fitness effects
1305 by counting the number of mutants arising with selection coefficients in the interval [s, s+ds]
1306 across the course of the evolution experiment. To infer a rate, we adjust the amount of time that
1307 this mutant could have arisen and been detected based on the mean fitness of the population,
1308 the time it takes for the mutant to establish, and its ability to rise to a detectable frequency in the
1309 population. Specifically, the number of mutations in the interval [s, s+ds] is expected to be:
1310

$$1311 \text{number of mutations in } ds = \mu(s)ds \times (s/c) \times N_e \int_0^{t-(1/s)\ln(n_0s/c)} e^{-\bar{x}(t)} dt$$

1312

1313 Where $N_e = 7 \times 10^7$ is the effective population size, $\bar{x}(t)$ is the mean fitness of the population
1314 over time, $c \sim 3.5$ is the offspring number variance, and $n_0 \sim 1000$ is the effective lineage size. We
1315 invert this function to estimate $\mu(s)$.

1316

1317 **Counting barcodes and calculating fitness from fitness measurement sequencing data**

1318 We used BarcodeCounter2 (Venkataram et al. 2016; *BarcodeCounter2: Count DNA Barcodes*
1319 *Version 2*, n.d.) to assign reads to their associated samples and barcodes. Briefly, we extracted
1320 the inline index, barcode, and UMI regions from each read using BLAST (Altschul et al. 1990) to
1321 the known constraint region in the amplicon sequence. Then, we associated each read to its
1322 corresponding condition and timepoint based on its combination of Illumina and inline indices.
1323 We then used Bowtie2 (Langmead and Salzberg 2012) to map the extracted barcode regions to

1324 our known list of barcodes in the experiment, used UMIs to avoid over-counting duplicate reads,
1325 and counted the number of barcodes per sample.

1326
1327 To infer fitness values, we used the fitness inference procedure as developed previously. In
1328 each time interval, a mutant's fitness is calculated as it's log-frequency change, adjusted by the
1329 mean fitness of the population. We infer the mean fitness of the population by calculating the
1330 log-frequency change of the set of 60 neutral lineages from Venkataram 2016.

1331

1332

1333 **Frequency dependence**

1334 During the analysis of the fitness measurement data, we noticed a systematic shift of fitness
1335 over the course of the experiment, with many barcoded mutants showing a decline in fitness
1336 fitness in 1- and 2-Day experiments as the fraction of the population that was adaptive
1337 increased, even after adjustment for changes in mean fitness (Figure S1). These trends were
1338 not identified in previous experiments, and we suspect that this is due to frequency-dependent
1339 fitness effects driven by the very strongly adaptive mutants. To avoid the influence of these
1340 effects, we used only the first timepoint interval from 2-Day experiments (from timepoint 0 to
1341 timepoint 1), as this kept our fitness measurements consistent with previous studies [cite
1342 Kinsler, Li]. Throughout the rest of the study, 2-Day fitness refers to this measurement using
1343 only early timepoints.

1344

1345 **Quantifying performances**

1346
1347 To quantify mutant performances in each phase of growth, we quantified differences between
1348 fitnesses inferred from 1-, 2-, 3-, and 5-Day transfer experiments. Because the time interval
1349 between 24 and 48 hours only contains respiration phase, we quantified respiration
1350 performance per hour as:

$$1351 \text{ResPerHour} = \text{2-Day fitness} - \text{1-Day fitness} / 24\text{hrs}$$

1352

1353 To calculate fermentation performance, we removed the 4 hours worth of respiration
1354 performance from the 1-Day fitness and divided the remaining fitness into the 16 hours of
1355 fermentation performance (accounting for ~4 hours of lag phase):

$$1356 \text{FerPerHour} = (\text{1-Day fitness} - 4 * \text{ResPerHour}) / 16\text{hrs}$$

1357

1358 Because 1-Day fitness measurements are used for both respiration and fermentation
1359 performances, there is the potential for noise in 1-Day measurements to introduce a relationship
1360 between fermentation and respiration performances. To eliminate measurement noise from
1361 having this influence, we used different replicates of the 1-Day fitness to calculate fermentation
1362 and respiration performance. Specifically, we used the replicate 2 flasks to calculate respiration
1363 performance and the replicate 1 flasks to calculate fermentation performance.

1364

1365 To infer stationary phase performance, we took the difference between 5- and 3-day fitness and
1366 divided by 48hrs of time:
1367 StaPerHour = (5-Day fitness - 3-Day fitness) / 48hrs
1368
1369 To calculate the uncertainty of performances, we used error propagation from the estimated
1370 errors of fitness. To calculate performances relative to parental strain, we computed the
1371 difference between each mutant's performance and its parental strain. For *CYR1*, *GPB2*, *TOR1*,
1372 and *IRA1-missense* second-step mutations, we used the mean of the neutral barcode strains as
1373 the parental reference measurement. For *IRA1-nonsense* second-step mutations, for which no
1374 neutral clones were isolated, we used the parental barcoded barcoded mutant present in the
1375 pool of first-step mutants (denoted with a "+" in main text figures).
1376
1377 **Differences in selection pressure do not drive the shift towards modular adaptation**
1378
1379 To evaluate whether a systematic shift in selection pressure occurred during the second-step
1380 evolution experiments, we identified mutants for which we called their evolution fitness from the
1381 estimation of the distribution of fitness effects. Because many of the remaining mutants are pure
1382 diploids whose spread may be dominated by measurement noise, we removed these mutants
1383 from the list. This resulted in a set of 185 second-step mutants. We then performed a partial
1384 correlation analysis between respiration performance and evolution fitness, accounting for
1385 fitness measurement fitness. We find no evidence of such a relationship ($p=0.74$, $r=-0.02$).
1386 Similarly, we find no relationship between fermentation performance and evolution fitness after
1387 accounting for fitness measurement fitness ($r=0.38$, $p=0.613$).
1388
1389 **1-Day evolution experiment analysis**
1390
1391 To evaluate whether yeast adapting to a 1-Day transfer could further improve their fermentation
1392 performance, we quantified the performance of 1-Day mutants as above. We identified several
1393 mutants with fermentation performances meeting or exceeding the maximum fermentation
1394 performance achieved by first-step mutants. Using a threshold of at least 2 standard errors
1395 (which corresponds to a FDR of $p<0.05$) a single second-step mutant that arose in the Evo1D
1396 *IRA1-nonsense* population had fermentation performance that exceeded the first-step
1397 maximum.
1398
1399 **Whole genome sequencing**
1400 We selected mutants for whole genome sequencing based on their fitness and performance in
1401 the growth phase, such that we selected as many unique mutants as possible based on their
1402 performances and those that had barcodes confidently identified by the metagrid. This resulted
1403 in a total of 346 clones targeted for sequencing.
1404
1405 Clones that were selected for sequencing were grown in 500 μ L of YPD in 96-well deep well
1406 plates for 2 days at 30°C without shaking. 400 μ L of saturated culture was collected from each

1407 well for genomic DNA extraction using the Invitrogen PureLink Pro 96 Genomic DNA Kit.
1408 Libraries were prepared using a 1/5 dilution protocol of the Illumina DNA prep, using Illumina
1409 Unique Dual Indexing primers.

1410

1411 **Variant calling**

1412 To identify variants from the sequencing data, we used bwa (H. Li and Durbin 2009) to align all
1413 reads to the S288C reference genome (R64-1-1-20110203). We then used picard
1414 (<https://broadinstitute.github.io/picard/>) to fix read groups and marked duplicate reads. We then
1415 used GATK (version 4.2.0.0) (Van der Auwera and O'Connor 2020) to generate individual
1416 GVCF files, merge GVCF files, and call genotypes on all samples. After removing samples with
1417 less than 20x coverage, we removed variants according to the following filters: QD < 5, FS < 60,
1418 SOR < 3, M! < 50, MQRankSum < -3.0, ReadPosRankSum < -5.0. After this filtering, we further
1419 removed ancestral variants present in all samples, mitochondrial variants, variants with GQ less
1420 than 70. This filtering resulted in 727 sites that were variable across our samples. We then
1421 manually inspected all called variants, resulting in 631 manually verified variants. We then used
1422 bcftools (H. Li 2011) to filter the vcf file to these verified variants and used snpEff (Cingolani et
1423 al. 2012) to annotate variants.

1424

1425 We then assigned variants to the corresponding barcoded mutants based on plate position. To
1426 check that our assignment was correct, we also verified the barcodes from the whole genome
1427 sequencing reads. For the 326 mutants for which we had sufficient coverage of the barcode
1428 region (at least 4 successfully-mapped barcode reads), 324 had the correct barcode identified.
1429 We opted to not use sequencing information from the 2 samples with mismatching barcodes
1430 between the sequencing and expected based on clone isolation barcode sequencing.

1431

1432 We further identified pre-existing mutations in which identical mutations were present in several
1433 sequenced mutants of a given low-complexity barcode. These mutations were classified as
1434 “pre-existing” mutations and ignored in downstream analyses except in cases where they
1435 belonged to a putatively causal gene (see “Mutation and ploidy classification” section).

1436

1437 **Mutation and ploidy classification**

1438

1439 To identify mutations likely responsible for driving fitness gains in these experiments, we
1440 identified putative adaptation-driving mutations by identifying mutations that occurred in genes
1441 that were recurrently mutated across adaptive clones. Specifically, genes with 4 or more
1442 mutations were classified as likely adaptation-driving. After classifying genes based on their
1443 function, we further identified additional mutations as adaptation-driving due to their effect on
1444 similar processes as recurrently mutated genes.

1445

1446 To classify the ploidy of mutations, we initially classified mutants according to their performance
1447 in the benomyl assay. We additionally classified mutants as “pure diploids” and “neutral
1448 haploids” by their similarity to the large cluster of haploids and diploids in terms of their fitness

1449 effects across all the conditions. Mutants that were within this large cluster of diploids but initially
1450 classified as haploids according to the benomyl assay were classified as pure-diploids.

1451
1452 From this initial ploidy classification, the majority of mutants which exhibited mutations in *PAB1*
1453 were classified as diploids, perhaps reflecting a sensitivity of *PAB1* mutants to benomyl. We re-
1454 classified all *PAB1* mutants as adaptive haploids with respiration performance relative to
1455 parental strain less than 0.06. *PAB1* mutants with greater respiration performance were
1456 classified as high-fitness diploids, consistent with the effect that auto-diploidization had on
1457 mutations from other genes. Similarly, *PAN2* and *PAN3* mutants were classified as diploids and
1458 have previously been shown to be susceptible to benomyl (Brown et al. 2006). Given we had
1459 few of these mutations, we did not have enough information to reclassify these mutations as we
1460 did for *PAB1*.

1461

1462 **Data availability**

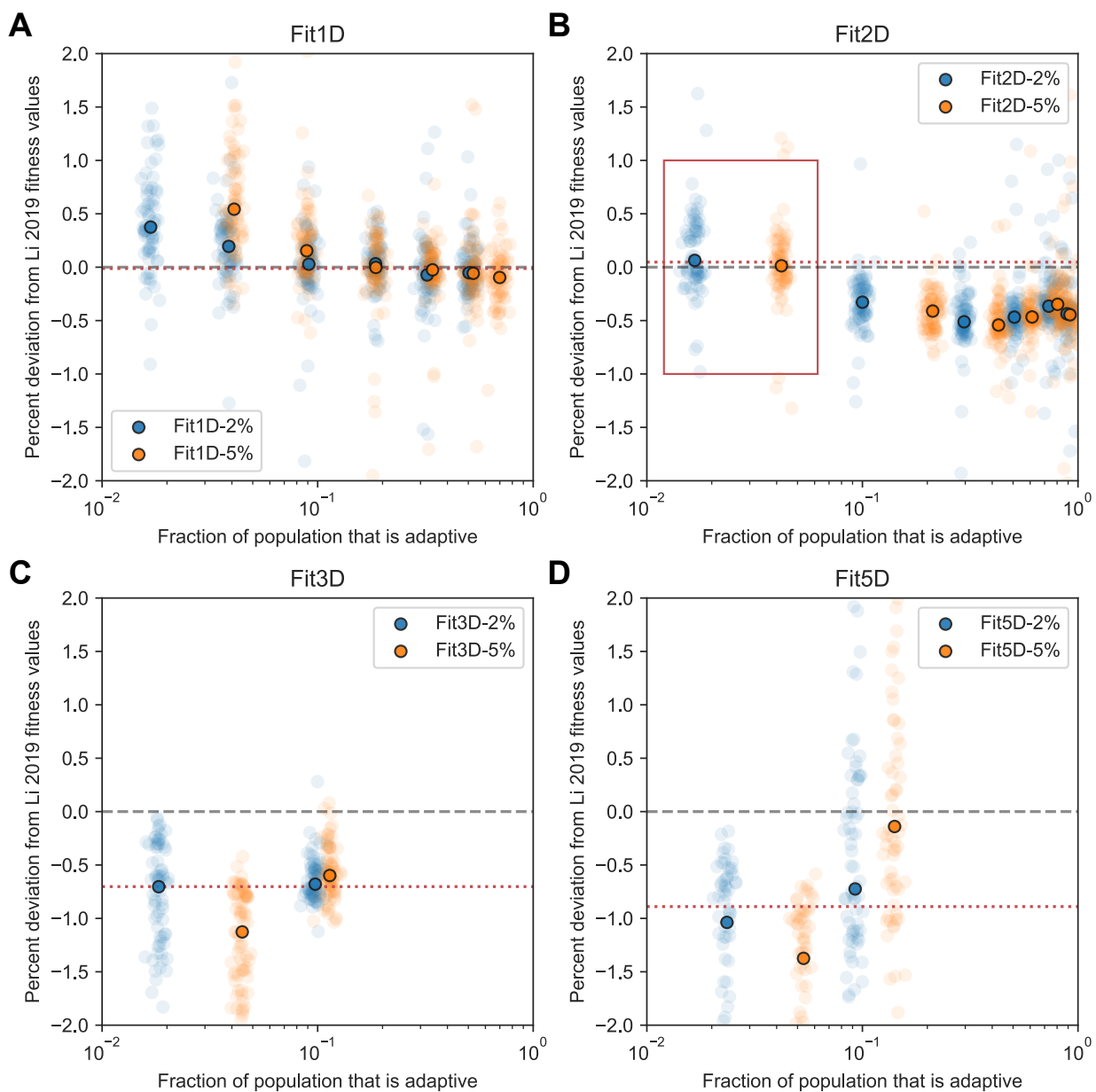
1463 Raw sequencing data is available on Short Read Archive under BioProject Number:
1464 PRJNA1098711. Processed frequency counts, fitness data, performance data, and mutational
1465 calls are available on Github: <https://github.com/grantkinsler/EvolvingFront>. All yeast strains are
1466 available upon request.

1467

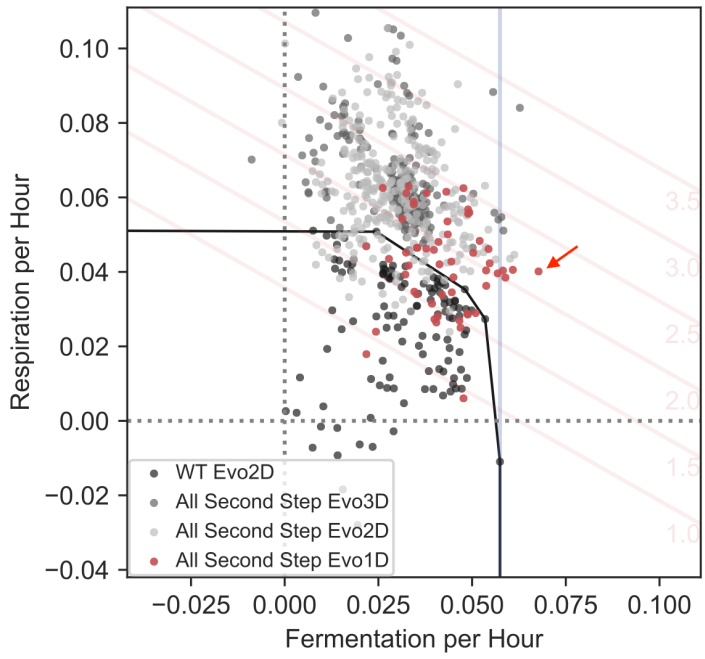
1468 **Code availability**

1469 Code for all data processing and figure generation is available on Github:

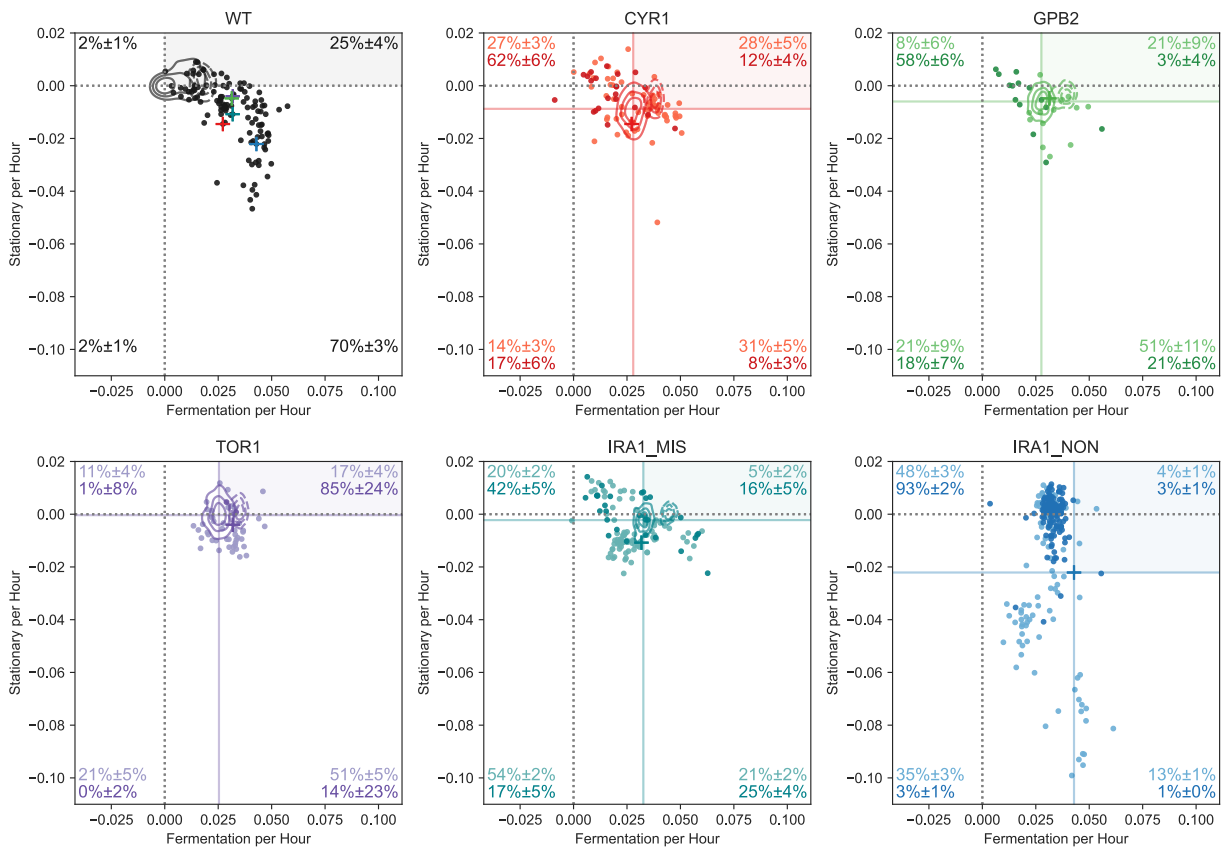
1470 <https://github.com/grantkinsler/EvolvingFront>

SUPPLEMENTARY FIGURES

1473 **Fig S1. Evidence for frequency dependence in fitness measurement experiments.** The
 1474 vertical axis of each subplot depicts the percent deviation from Li 2019 fitness values for the set
 1475 of adaptive haploids that were present in Li 2019 fitness measurements and this study. The
 1476 horizontal axis is the fraction of the population that is adaptive. Points show the deviation for
 1477 each mutant, with the median across all mutants depicted by the heavy circle. Blue and orange
 1478 points are from experiments initiated with the adaptive barcode pool consisting of 2% and 5% of
 1479 the population, respectively. Red dotted line indicates the deviation for the overall fitness
 1480 measurement used throughout the paper. Red box in (B) refers to the timepoints used.
 1481 Subpanels A-D refer to Fit1D, Fit2D, Fit3D, and Fit5D fitness values, respectively.

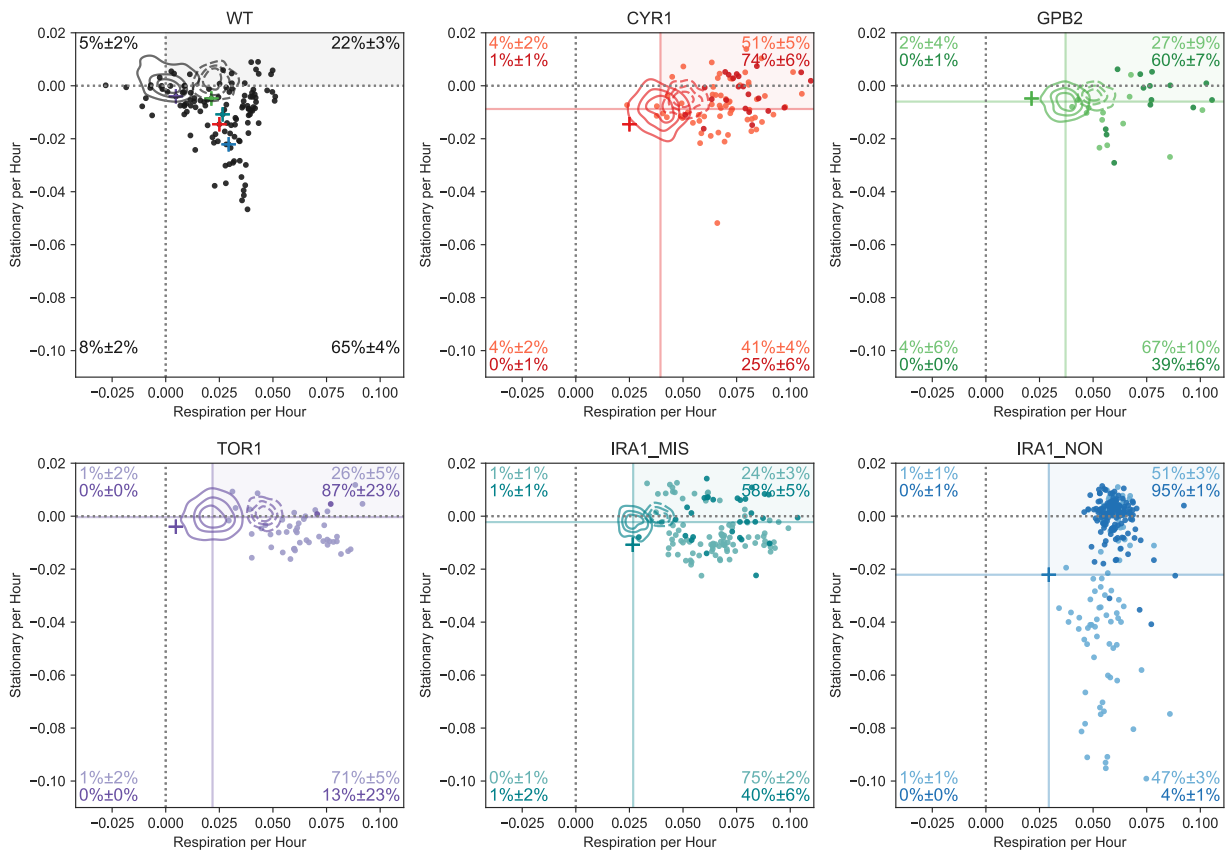


1482 **Fig S2. 1-Day evolution experiments identify mutants that improve fermentation**
 1483 **performance.** Fermentation and respiration performances for mutants discussed in the main
 1484 text and Evo1D mutants (in red). Despite less dense sampling, we find at least one Evo1D
 1485 mutant (indicated with red arrow) with fermentation performance that exceeds the highest
 1486 fermentation performance from first-step mutants (blue vertical line).



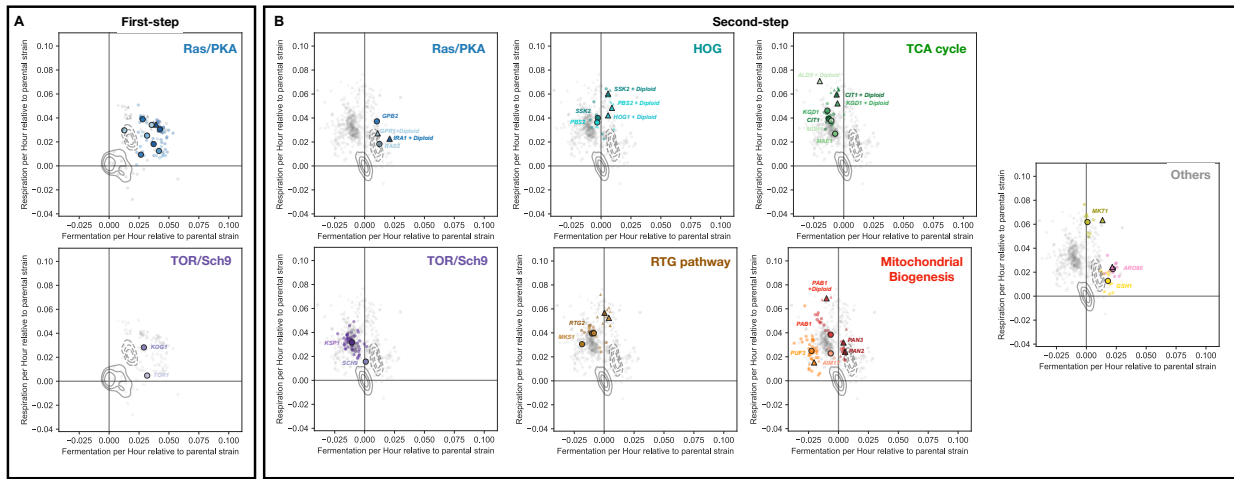
1487

1488 **Fig S3. Fermentation and stationary phase performances by parental strain.** Each
 1489 subpanel depicts a scatter plot with the fermentation and stationary performances for each
 1490 parental strain. Lighter points indicate Evo2D mutants, darker points indicate Evo3D mutants.



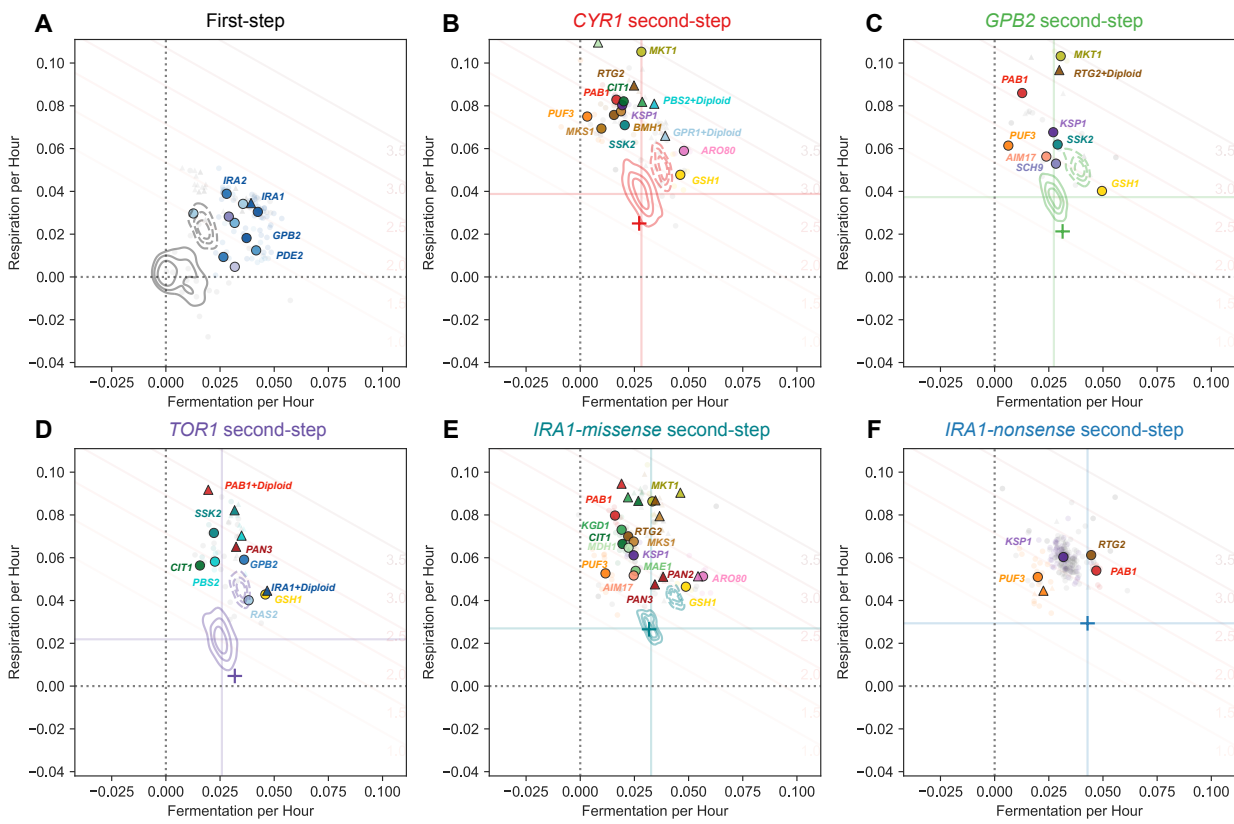
1491
1492
1493
1494

Fig S4. Respiration and stationary phase performances by parental strain. Each subplot depicts a scatter plot with the respiration and stationary performances for each parental strain. Lighter points indicate Evo2D mutants, darker points indicate Evo3D mutants.



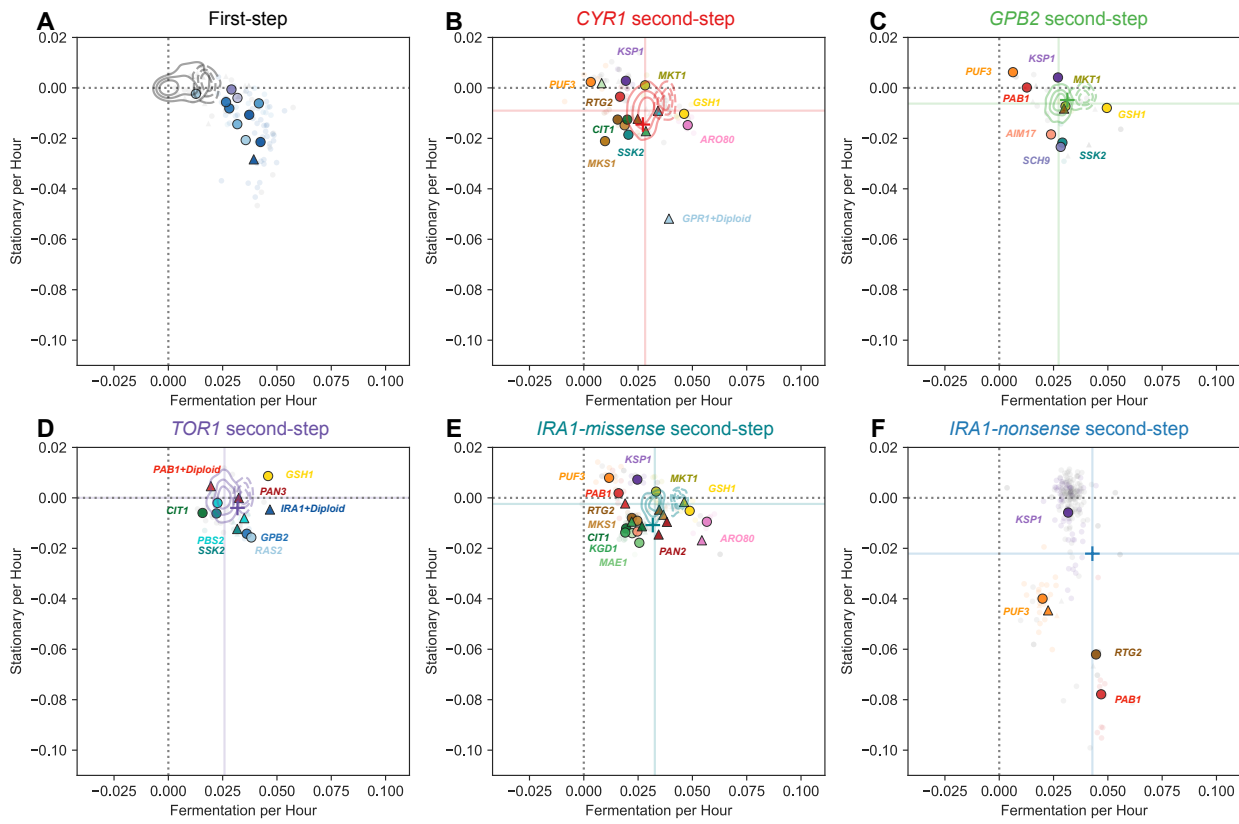
1495
1496
1497
1498
1499
1500
1501

Fig S5. Molecular targets of adaptation by gene. Performance effects of mutations separated by biological process or pathway as in Table 1. Points are colored by gene, and shape indicates ploidy (circles are haploids, triangles diploids). KDE estimates show density of neutral haploids for each parental strain (solid lines) and pure diploids for each parental strain (dashed lines). **(A)** First-step mutants. **(B)** Second-step mutants depicted, with performances measured relative to parental strain.



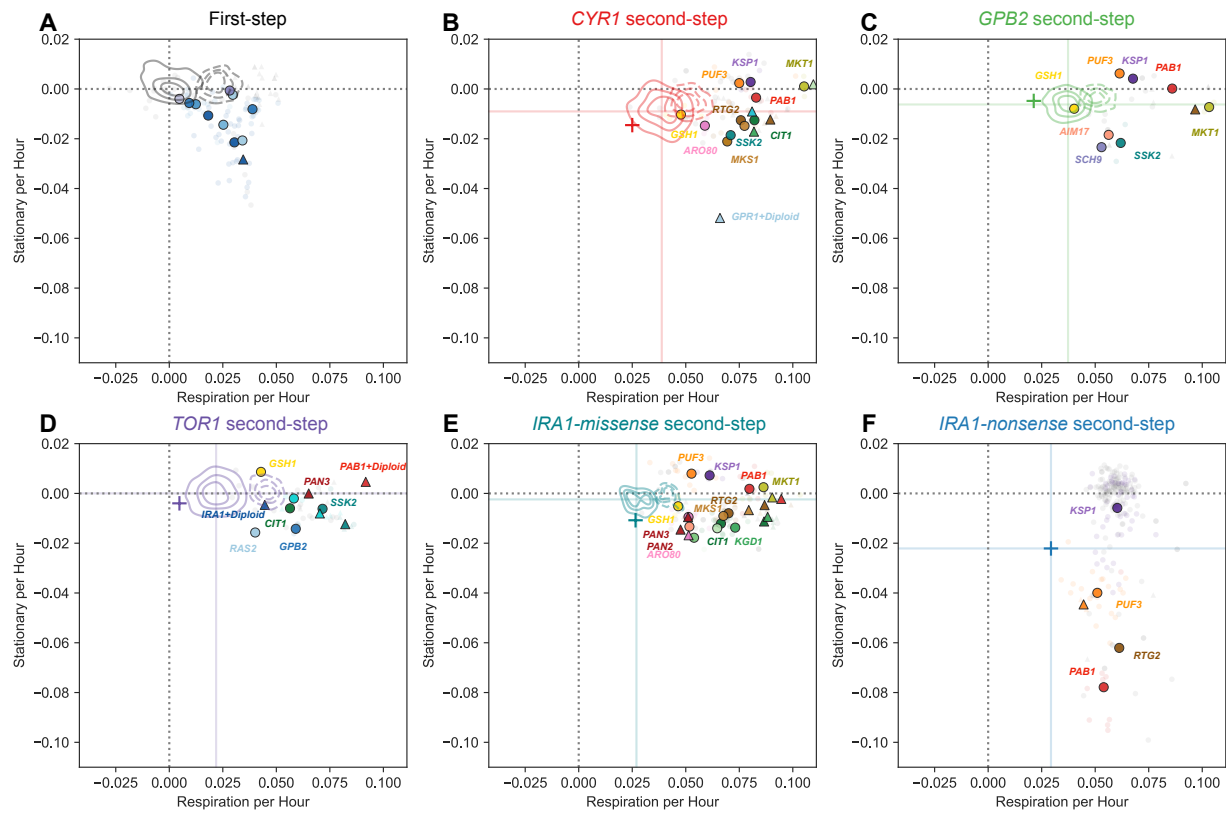
1502
1503
1504
1505

Fig S6. Molecular targets of adaptation by gene. Colored by gene, shape depicts ploidy (circles are haploids, triangles diploids). KDE estimates show density of neutral haploids for each parental strain (solid lines) and pure diploids for each parental strain (dashed lines).



1506
1507
1508
1509
1510

Fig S7. Mutational effects on fermentation and stationary phase performance. Colored by gene, shape depicts ploidy (circles are haploids, triangles diploids). KDE estimates show density of neutral haploids for each parental strain (solid lines) and pure diploids for each parental strain (dashed lines).



1511
1512
1513
1514
1515

Fig S8. Mutational effects on respiration and stationary phase performance. Colored by gene, shape depicts ploidy (circles are haploids, triangles diploids). KDE estimates show density of neutral haploids for each parental strain (solid lines) and pure diploids for each parental strain (dashed lines).